ISSN 1345-3041
MITSUBISHI ELECTRIC Dec. 2006／Vol.116

ADVANCE

The State of the Art and Future Trends in Electromagnetic Actuation Technology

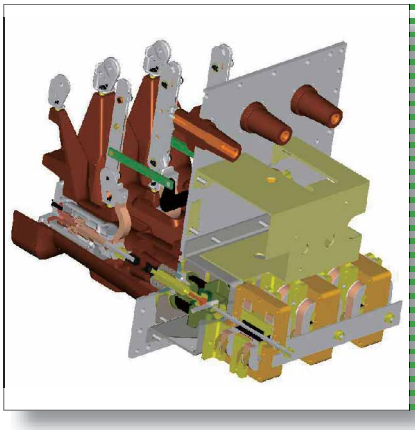

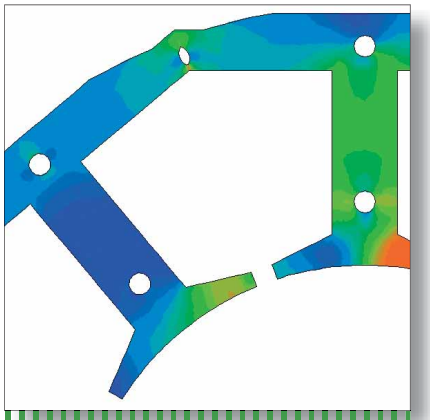

$$I_{coil}(t)\cdot(R_{coil}+R_{out})+\frac{d\phi(I_{coil}(t),z(t))}{dI_{coil}}\frac{dI_{coil}(t)}{dt}+\frac{d\phi(I_{coil}(t),z(t))}{dz}\frac{dz}{dt}=E$$

$$m(z(t))\frac{d^2z}{dt^2}=Fm(I_{coil}(t),z(t))+Fs(z(t))+F_{friction}$$

Electromagnetic Analysis Coupled with Motion

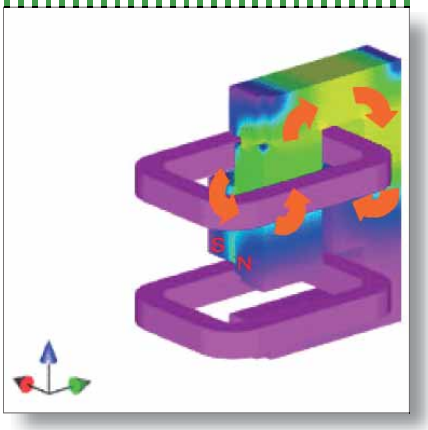

MITSUBISHI ELECTRIC
Changes for the Better

Dec. 2006 / Vol. 116
MITSUBISHI ELECTRIC
ADVANCE
The State of the Art and Future Trends in Electromagnetic Actuation Technology

Cover Story

Shown on the cover are examples of products and their construction employing electromagnetic actuation technology. Shown on the right are EGR (exhaust gas recirculation) motors and the results of electromagnetic-field analysis performed on them, while shown on the left is power switchgear and the results of electromagnetic-field analysis of its electromagnetic actuators.

• **Editorial Inquiries**
Hisao Okamoto
Corporate Total Productivity Management
& Environmental Programs
Fax +81-3-3218-2465

• **Product Inquiries**
Yoshikazu Ishii (p11-13, p20-28)
Design System Planning Section
Manufacturing Systems Planning Dept.
Nagoya Works
Fax +81-52-723-1131

Keiichi Itoh (p1-10, p14-19)
Electromagnetic Machine Group
Electromechanical Systems Dept.
Advanced Technology R&D Center
Fax +81-6-6497-7288

Mitsubishi Electric Advance is published on line quarterly (in March, June, September, and December) by Mitsubishi Electric Corporation.

CONTENTS

Technical Reports

Overview

Author: *Kenichi Koyama**

Products that are designed to actuate something using electricity are required to convert electric energy into kinetic energy, and therefore often take advantage of an electromagnetic phenomenon. Many of the products manufactured by Mitsubishi Electric Corporation employ motors and electromagnetic actuator, both of which capitalize on electromagnetic effects. These products or equipment are required to deliver enhanced efficiency in order to reduce carbon dioxide emissions. At the same time, there is growing demand for increased speed and greater precision in order to provide such products with higher added value.

With this background, we have been conducting basic research in order to clarify electromagnetic effects, and thus design and develop sophisticated electromagnetic drive equipment utilizing basic principles. In addition to developing systems using electromagnetic drive equipment, we have been developing technologies for mass-producing products while retaining high performance and stability.

As a result, each year we have successfully increased the drive efficiency of our motors for industrial equipment and motor vehicles, while enhancing the controllability of those motors. Furthermore, for the actuation of contacts in power switchgear, we have developed a new technology dubbed an “electromagnetically actuated mechanism”.

Going forward, we are determined to meet the needs of our customers by innovating our electromagnetic drive technology in the field of electric energy conversion while actively helping to protect the Earth's environment.

**Advanced Technology R&D Center*

Electromagnetic Actuator Design Technology Using Electromagnetic Coupled with Motion Analysis

Author: *Toshie Takeuchi**

Mitsubishi Electric's 15 kV rated high-speed switchgear and SF6-gas-free insulation (dry-air gas insulation) switchgear employ direct-drive electromagnetically actuated vacuum circuit breakers in place of conventional spring-operated circuit breakers.

We developed an electromagnetic and motion-coupled analysis method capable of precisely simulating the dynamic behavior of vacuum circuit breakers and applied the method to develop the above-mentioned circuit breakers.

1. Drive design technology for eddy current repulsion high-speed switches using equivalent circuit method

First, the electromagnetically actuator design technology applied to Mitsubishi's 15 kV rated high-speed switch is shown in Fig. 1[(1)]. The high-speed switch is a circuit breaker that has performance values such as an opening time of about 1 ms and a breaking time of 1 cycle or less. Compared with general circuit breakers that feature an opening time of about 25 ms, this switch has a much faster response. The high-speed switch is used for high-speed switching units in power receiving systems or private power generation systems, and is attracting the attention of industry today for protecting important power loads in the event of a momentary power failure.

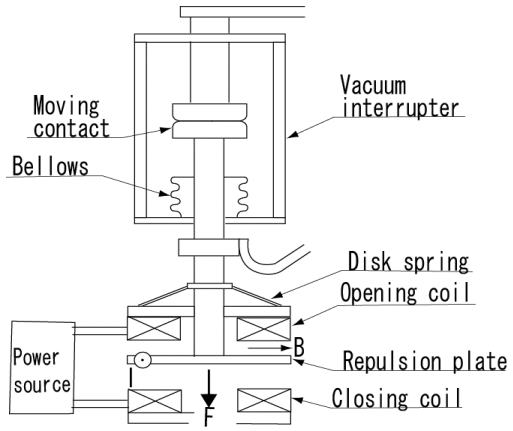

Fig. 1 Diagram of single phase of high speed switch

Mitsubishi's high-speed switches consist of a vacuum interrupter that contains a contact member to open or close the circuit, a coned disc spring having a nonlinear loading characteristic, and an electromagnetic repulsion mechanism which includes a repulsion plate of low resistance between the upper and lower fixed coils for opening and closing operation. For example, for opening, the coil supplied with pulsed current helps induce electromagnetic repulsive force in the repulsion plate to start opening the contact within 1 ms of the opening time. In order to design the electromagnetic repulsion drive mechanism to speed up the response with as small a pulse power supply as possible, it was necessary to conduct a coupled analysis involving transient electromagnetic field analysis containing a pulsed power supply circuit and a motion with nonlinear loading characteristic considered.

By simulating induction current with the use of one-turn imaging coil having a skin depth of δ and then applying it to the inductively coupled equivalent circuit shown in Fig. 2, we developed an electromagnetic analysis method coupled with a motion equation considering a non-linear spring[(1)]. The method using an equivalent circuit approach does not require the mesh that is usually necessary for an FEM and allows shape parameters to be easily changed; the method is useful for a model that does not use non-linear material, for example 15 kV rated high-speed switches, and is also suitable for combination with an optimization method.

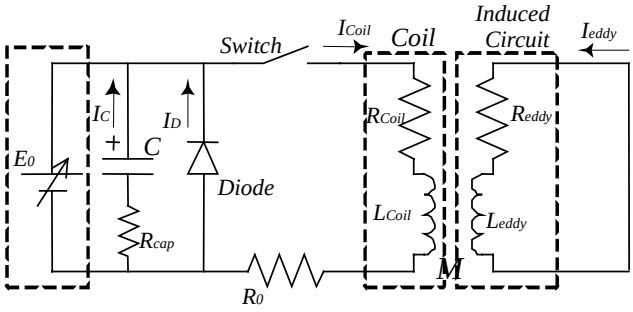

Fig. 2 Electric equivalent circuit

Next, look at the formulation of the equivalent circuit shown in Fig. 2. The electric circuit on the fixed coil side is an LCR circuit until the capacitor starts to discharge and Eqs. (1) and (2) are established using the mutual inductance *M* with respect to the inductive circuit. In the equations, $d\phi_{eddy}/dt$ and $d\phi_{coil}/dt$ are changes in

**Advanced Technology R&D Center*

interlinked flux due to the motion of the repulsion plate. Assuming the direction of the motion is represented by "χ", Eqs. (3) and (4) are formulated.

$$\frac{q}{C} + Icoil(Rcoil + Rc) + Lcoil\frac{dIcoil}{dt} - M\frac{dIeddy}{dt} + \frac{d\phi_{eddy}}{dt} = 0 \quad (1)$$

$$Ieddy \cdot Reddy + Leddy\frac{dIeddy}{dt} - M\frac{dIcoil}{dt} + \frac{d\phi_{coil}}{dt} = 0 \quad (2)$$

$$\frac{d\phi_{eddy}}{dt} = -\frac{dM}{dx}\frac{dx}{dt}Ieddy \quad (3)$$

$$\frac{d\phi_{coil}}{dt} = -\frac{dM}{dx}\frac{dx}{dt}Icoil \quad (4)$$

Then, the electromagnetic force *Fm* generated in the inductive coil can be expressed by Eq. (6) below, based on the concept of virtual displacement, with magnetic energy assumed to be *Em*. It represents the electromagnetic force generated in the repulsion plate. From this electromagnetic force, the equation of motion (7) is formulated so that it can be coupled with the electric circuit equations (1) through (4) above for solution.

$$Em = M \cdot Icoil \cdot Ieddy \quad (5)$$

$$Fm = \frac{dEm}{dx} = -\frac{dM}{dx}Icoil \cdot Ieddy \quad (6)$$

$$m\frac{d^2x}{dt^2} = Fm + Fs + F_0, Fs = k(x - x_0) \quad (7)$$

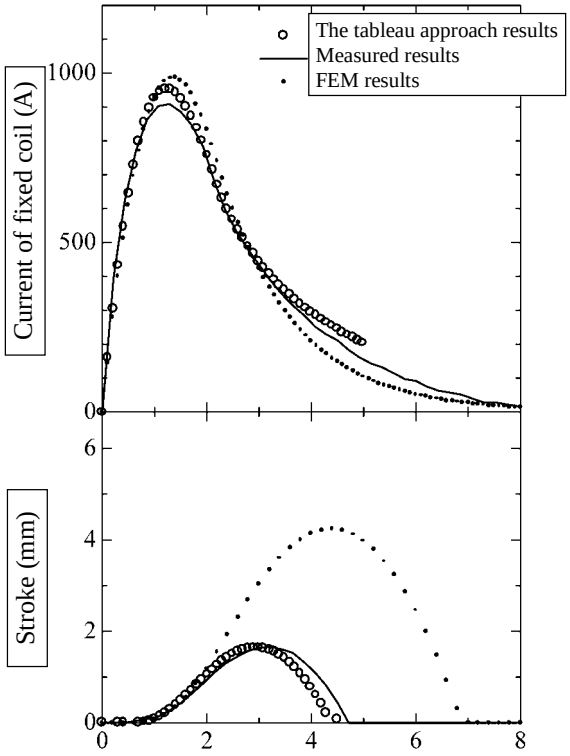

Fig. 3 Results of currents on fixed coil and strokes of repulsive plate

where *m* is the mass of the movable part, χ the position of the movable part, *Fs* the spring force, *F0* certain force other than spring force, *k* the equivalent spring constant, and x0 the position of the movable part at a natural length of spring.

Figure 3 shows a comparison between the results of the combination analysis using the equivalent circuit method discussed above and the results of measurement. The values of the analysis results and measurements are in good agreement, indicating that the use of this analysis method can improve the technologies required for designing the driving elements of the circuit breakers.

2. Drive design technology for electromagnetically actuated vacuum circuit breaker

The following section describes the drive design technologies for the electromagnetically actuated vacuum circuit breaker developed for 24 kV rated SF6-gas-free insulation (dry-air gas insulation) switchgear that was introduced in the market in 2004 [2].

Figure 4 shows a schematic drawing of the structure of the developed electromagnetically actuated vacuum circuit breaker. In this circuit breaker, Mitsubishi Electric's original high-efficiency electromagnetic actuation mechanism replaces the conventional spring mechanism.

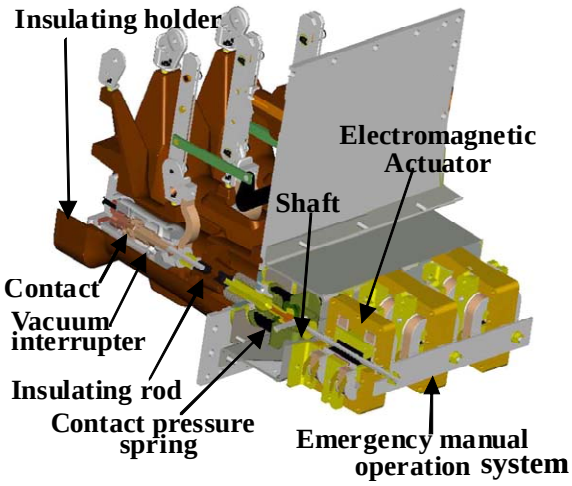

Fig. 4 Structure of 24kV rated VCB

With the number of components in the mechanism reduced for enhanced reliability, there are fewer wearable parts such as latch levers, etc. and no need for greasing the parts, realizing maintenance-free performance. Furthermore, a vacuum interrupter, insulating rod, contact pressure spring, and bistable electromagnetic actuator are arranged in a straight line for each phase, thus eliminating the three-phase link mechanism and incorporating a direct-drive independent phase driving method. The use of the independent phase

driving method also allows extension of a synchronous circuit breaker as well as a general-purpose circuit breaker. The electromagnetically actuated mechanism is simply structured, consisting of the first fixed lamination yoke, second fixed lamination yoke, permanent magnet, laminated plunger, and opening and closing coils. The number of parts used in the mechanism is reduced by 35% compared to the conventional type. Open and close holding operation completes by means of the permanent magnet, without requiring any electric energy consumption; the opening and closing coils are respectively actuated by the current discharged from the capacitor circuit. The use of the second yoke, which is an original design of Mitsubishi Electric, separates the magnetic path of the permanent magnet from the magnetic path of the excitation coil for highly improved efficiency of opening and closing operation. Furthermore, the plunger has also been laminated for minimized eddy current during its operation.

For realizing 3-phase simultaneous open-close control by employing the 3-phase independent driving method, the operation variation between the three phases must be limited to several ms or less. For that purpose we developed a drive design technology using transient electromagnetic and motion-coupled analysis capable of precisely calculating the dynamic behavior of circuit breakers. With this method, the dependency on current and plunger position (stroke) of the flux ϕ (I, z) and magnetic force Fm (I, z) was determined by 3-D static electromagnetic field analysis and analyzed with Eqs. (8) and (9) coupled. The delay of magnetic flux and magnetic force by the eddy current in the electromagnetic actuation mechanism is expressed by Eqs. (10) and (11) using time constant τ. The time constant τ was determined based on the results of the driving test of the electromagnetic actuator in the form of a single unit. The discontinuity of changes in the strength of the contact-pressure spring and mass of movable part was solved by applying the law of conservation of momentum. Figure 5 shows the results of this analysis and the results of measurement made on the circuit breaker as a single unit. Figure 5 clearly indicates that the accuracy of the analysis has been remarkably improved by the application of the time constant τ and the law of conservation of momentum. We have optimized the design of the electromagnetic actuation mechanism by using this method and achieved an efficiency that could be referred to as one of the highest levels in the world as the driving energy is reduced to 20% of that of a conventional VCB by Mitsubishi Electric.

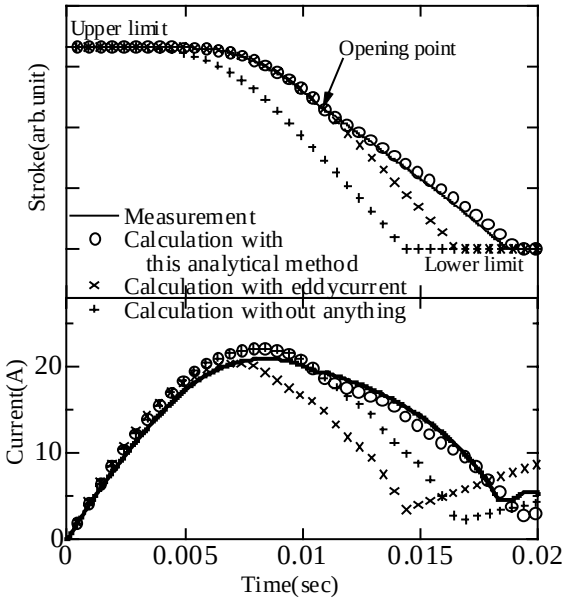

Fig. 5 Calculated and measured strokes and currents on the opening operation

The method that we developed does not require updating of the mesh, unlike the FEM method, and can reduce the calculation time to one-tenth of the conventional method. Virtual design of operation time differences due to manufacturing and assembly control tolerances is now possible from the desktop, with the result that the design requirements for limiting the operation variations between the three phases to several ms were easily extracted. Mitsubishi Electric's 24 kV rated SF6-gas-free insulation (dry-air gas insulation) switchgear was introduced ahead of any other competitors in the world and won the 2005 Japanese Award for Outstanding Achievement in Industrial Technologies (Promotion Prize).

$$\frac{q(t)}{C} + I_{coil}(t)\cdot(R_{coil}+R_{out}) + \frac{d\phi(I_{coil}(t),z(t))}{dt} = E,\ \frac{dq(t)}{dt} = I_{coil} \quad (8)$$

$$m(z(t))\frac{d^2z}{dt^2} = Fm(I_{coil}(t),z(t)) + Fs(z(t)) + F_{friction} \quad (9)$$

$$\phi_{transient} = \phi_{static}(I_{coil}(t)(1-\exp(-\tau t)),z(t)) \quad (10)$$

$$Fm_{transient} = Fm_{static}(I_{coil}(t)(1-\exp(-\tau t)),z(t)) \quad (11)$$

References

(1) ToshieTakeuchi, et al.: "Electromagnetic Analysis Coupled with Motion for High Speed Circuit Breakers of Eddy Current Repulsion using the Tableau Approach", IEEJ Trans. PE, Vol. 124, No. 6, 2004, pp. 859-865

(2) ToshieTakeuchi, et al.: "An Electromagnetically Actuated Vacuum Circuit Breaker Developed by Electromagnetic Analysis Coupled with Motion", IEEJ Trans. PE, Vol. 124, No. 2, 2004, pp.321-326

Motor Design Technologies Considering Detailed Magnetic Properties in Magnetic Core

Author: *Akihiro Daikoku**

We investigated magnetic cores in practical use, focusing on detailed magnetic properties such as stress-induced deterioration from shrink-fitting the magnetic core to a frame, as well as magnetic anisotropy, in view of reducing the cogging torque in permanent magnetic servo motors. Then, we developed technologies based on magnetic analysis to quantify the cogging torque resulting from the magnetic properties mentioned above. Using a motor for verification, measurements and analysis were conducted to prove the validity of the developed technologies and their effectiveness in practical applications.

1. Motor Design Technology Considering Stress Distribution in Magnetic Core[1]

We developed a combination analysis system for structure and magnetic field to evaluate the influence of stress working on a magnetic core. Combination analysis is realized by providing each element of the magnetic analysis mesh with magnetic properties in accordance with the stress, based on the measured magnetic properties of electrical steel sheet under stress and the stress distribution obtained by structural analysis. This system is outlined below, the description of which assumes that the magnetic core is shrink-fitted to the frame.

(1) Magnetic properties of the magnetic core material under stress are measured.
(2) Structural analysis of the magnetic core shrink-fitted to a frame is conducted to determine the deformation and stress distribution in the magnetic core.
(3) FEM magnetic field analysis data is prepared based on the measurement results for the magnetic properties of the material and the results of structural analysis. First, a mesh of the magnetic core unaffected by the frame is prepared. Next, the mesh is deformed in accordance with the magnetic core deformation determined by the structural analysis. Then, property number values corresponding to stress values are allocated by reading the stress values at each element position from the results of the structural analysis.
(4) The property numbers are associated with the magnetization curve and then the magnetic field analysis are executed.

For stress values, either von Mieses stress (scalar value) or principal stress (vector value) is applicable in developed system.

We developed a magnetic property measuring device equipped with a stress-applying mechanism to measure the magnetic properties of electrical steel sheet under stress. Figure 1 shows the relationship between the relative permeability of 50A800 (JIS C 2552) and applied stress at the points where the magnetic flux density B = 1.0[T] and 1.5[T], as an example of measured results. When no stress is applied (0 [MPa]), the relative permeability is large; however, it decreases with increasing stress. The variation in relative permeability between tensile stress and compressive stress differs; the relative permeability decreases more rapidly in the case of compressive stress.

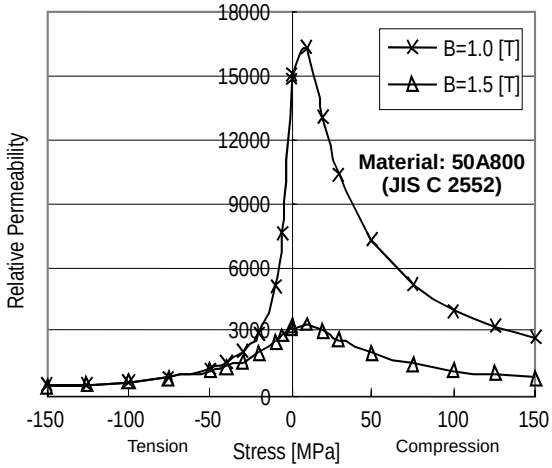

Fig. 1 Magnetic properties of electrical steel sheet under stress

Figure 2(a) shows a cross section of the motor for verification. The number of poles is 10, the number of slots 12, and the stator outer diameter, rotor outer diameter, and magnetic core length is 80, 35, and 39 mm, respectively. The material of the magnetic core is 50A800. Cogging torque analysis considering the stress generated inside the magnetic core as a result of

**Advanced Technology R&D Center*

shrink-fitting to the frame was conducted and the analyzed results are compared to the measured results. The frame is elliptic so that cogging torque arises noticeably. Figure 2(b) shows the model for magnetic field analysis considering von Mieses stress. The shade levels of the model elements represent respective property numbers dependent on stress values.

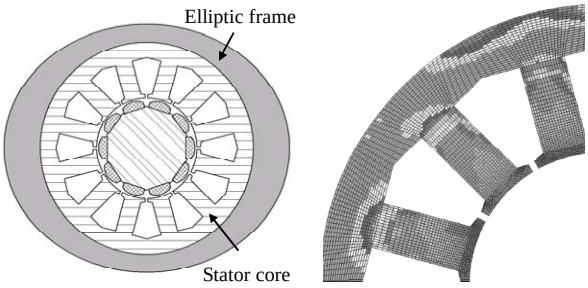

(a) Cross Section (b) Finite element mesh for magnetic field analysis considering von Mieses stress distribution.

Fig. 2 Cross section and finite element mesh of verification motor

Figure 3 shows the results of cogging torque analysis for different cases including those with von Mieses stress and deformation taken into consideration, with principal stress and deformation, and with deformation only, and the measured results. This figure clearly indicates that cogging torque arises due to both stress and deformation. The analyzed results agree well with the measured waveform in the case where principal stress and deformation are considered. In particular, the main pulsation component, which pulsates 10 times per rotation, indicates an error of about 4%, indicative of good agreement with the measured results.

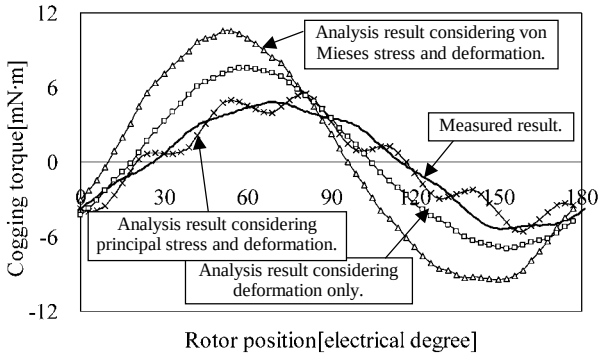

Fig. 3 Comparison of cogging torque waveforms resulting from stress

2. Motor Design Technology Considering Magnetic Anisotropy of Magnetic Core[2]

An electrical steel sheet, even if it is non-oriented, has magnetic anisotropy (difference in magnetic property depending on the direction) that must be evaluated in terms of influence on motor performance. In isotropic materials, the direction of magnetic flux density *B* and magnetic field strength *H* is the same. However, if anisotropic, *B* and *H* form a certain angle as shown in Fig. 4(a). Several methods are proposed for modeling magnetic anisotropy. In this study, the 2-D magnetic property method was employed. The amplitudes of *B* and *H*, "*B*" and "*H*", and the angles from the rolling direction, θ_B and θ_H, were used to express the permeability; accurate modeling using this method was achieved by reflecting the angle θ_{HB} between *B* and *H* just as it was actually measured. Figure 4(b) shows the measurement results for θ_{HB} on 50A290 by way of example.

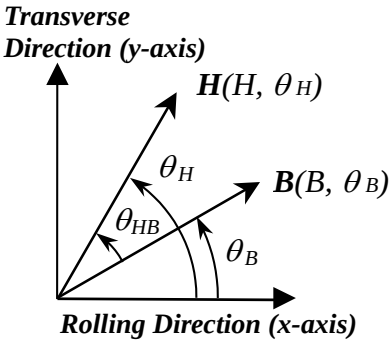

(a) Vector diagram

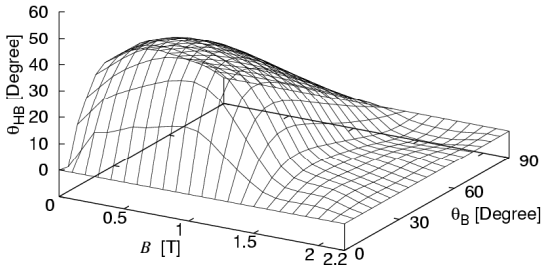

(b) Measured magnetic property of 50A290 (θ_{HB} to *B* and θ_B).

Fig. 4 2-D magnetic property

If stator core pieces are produced by punching a circular core out of an electrical steel sheet and they are stacked in such a way that all the rolling directions are aligned (parallel stacking), magnetic resistance will fluctuate twice or any number of times that is an integral multiple of 2 per rotation, due to magnetic anisotropy. Cogging torque is generated when the difference between the number of poles and the number of slots is equal to 2 with the parallel stacked magnetic core mentioned above. To eliminate this influence, core pieces can be stacked by rotating them one after another (rotational stacking). A typical example that renders remarkable influence from magnetic anisotropy is a motor with 10 poles and 12 slots, as with the case in the previous chapter. The cross section is the same as shown in Fig. 2(a), although the frame is removed. The

results of cogging torque analysis of a motor with anisotropic magnetic core and a motor with isotropic magnetic core were compared with the measured results for cogging torque on the magnetic cores of both parallel stacking and rotational stacking of a prototype, as shown in Figure 5. In the case of isotropic model or rotational stacking, the cogging torque pulsates 60 times per rotation, which is the least common multiple of the number of poles and number of slots. On the other hand, in the case of anisotropic model or parallel stacking, the cogging torque pulsates 10 times per rotation. The pulsation amplitudes of these cases agreed well, indicating that quantification is valid and effective.

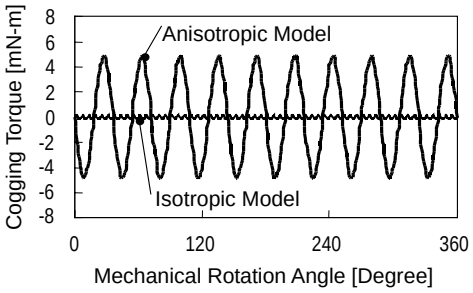

(a) Analyzed result

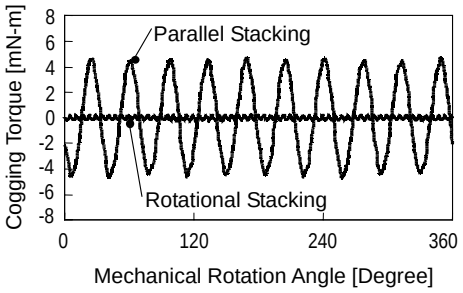

(b) Measured result

Fig. 5 Cogging torque waveforms with/without magnetic anisotropy

3. Future Prospects

We intend to further develop servo motors with reduced cogging torque by applying the developed motor design technologies discussed in this paper. The particular technologies are applicable to high-accuracy calculation of motor loss. We will also promote development of motors with enhanced efficiency by applying the developed technologies.

References

(1) A. Daikoku, et.al.: "An Accurate Magnetic Field Analysis for Estimating Motor Characteristics Taking Account of Stress Distribution in the Magnetic Core", IEEE *Transactions on Industry Applications*, Vol.42, No.3, pp.668-674(2006)

(2) S. Yamaguchi, et.al.: "Cogging Torque Calculation Considering Magnetic Anisotropy for Permanent Magnet Synchronous Motors", *COMPEL*, Vol. 23, No.3, pp. 639-646(2004)

Technologies of Magnetic Power Loss Analysis for Rotating Machines

Authors: *Haruyuki Kometani** and *Yoshihiro Tani**

In this report, methods for estimating magnetic power loss due to harmonic flux, and increased magnetic power loss resulting from deterioration of magnetic core material, are formulated for application to magnetic power loss analysis for inverter-driven motors, and are proved effective from the results of analysis.

The technologies discussed in this report are actually being applied to enhance the efficiency of permanent magnet motors for air-conditioner compressors, drives in factory automation systems, automobiles, railway system motors, and turbine generators.

1. Introduction

"High-efficiency motor" is one of the most important factors influencing product competitiveness in today's markets. With permanent magnet motors equipped with inverter drive systems, copper loss has successfully been reduced to the extreme by employing state-of-the-art technologies that include concentrated winding and interior permanent magnet structure. For further improved motor efficiency, reduction of magnetic power loss is indispensable. It is necessary to investigate the employment of high-efficiency materials for magnetic cores and the optimization of motor shapes and inverter specifications, aimed at reducing magnetic power loss, without the need for experimental manufacturing.

In this report, we discuss the new modeling methods we have developed, taking as an example their application to electromagnetic numerical analysis of magnetic power loss resulting from harmonics during inverter drive operation[1, 2].

2. Calculation Method for Magnetic Power Loss by High-frequency Flux[2]

For calculating the magnetic power loss of rotating machines, hysteresis loss, W_h, and eddy current loss, W_e, are calculated by conducting frequency analysis of the hysteresis of flux density, B, of each element obtained by electromagnetic numerical analysis and applying the result to the magnetic power loss curve after fitting[1].

$$W_h = \alpha B^{\gamma} f \tag{1}$$

$$W_e = \beta B^2 f^2 \tag{2}$$

where f is the frequency and α, β and γ are the constants obtained from the fitting curve.

When the frequency exceeds several kHz, becoming high frequency, flux and eddy current concentrate on the surface of the magnet core due to skin effect, which results in an increase in hysteresis loss and a decrease in eddy current loss. With the skin depth and average flux density in the magnet core sheet of defined as δ and B_0, respectively, the hysteresis loss is given by the equation below:

$$W_h = \frac{2}{t}\int_0^{t/2}\left(\alpha B^{\gamma} f\right)dx = \frac{2\alpha\delta f}{t\gamma}\left[\frac{B_0 t}{2\delta\left\{1-\exp\left(-\frac{t}{2\delta}\right)\right\}}\right]^{\gamma}\left\{1-\exp\left(-\frac{\gamma t}{2\delta}\right)\right\} \tag{3}$$

where t is the sheet thickness of the magnet core.

For an eddy current loss reduction coefficient κ, the eddy current loss is expressed as the following equation:

$$W_e = \beta B^2 f^2 \kappa \tag{4}$$

$$\kappa = \frac{6\left\{\left(\frac{3}{2}\delta+\frac{t}{2}\right)\exp\left(-\frac{t}{\delta}\right)+\frac{\delta}{2}-2\delta\exp\left(-\frac{t}{2\delta}\right)\right\}}{\left\{1-\exp\left(-\frac{t}{2\delta}\right)\right\}^2 t} \tag{5}$$

where the skin depth, δ, is defined by the following equation using the average flux density in the skin depth, B_{av}, and average magnetic field strength, H_{av}.

$$\delta = \sqrt{\frac{\rho H_{av}}{\pi f B_{av}}} \tag{6}$$

where ρ is the resistivity of the magnetic core. Then, B_{av} is given by the following equation:

*Advanced Technology R&D Center

$$B_{av} = \frac{B_0 t}{2\delta\left(1 - e^{-\frac{t}{2\delta}}\right)}\left(1 - \frac{1}{e}\right) \cdots\cdots \delta \le \frac{t}{2}$$
$$B_{av} = B_0 \cdots\cdots \delta > \frac{t}{2} \qquad (7)$$

Figure 1 shows a comparison between the magnetic power loss values obtained by the equations above and the measured values. The figure clearly indicates that the values of high-frequency magnetic power loss agree well with the measurements and suggests that the calculation method employed is valid and effective.

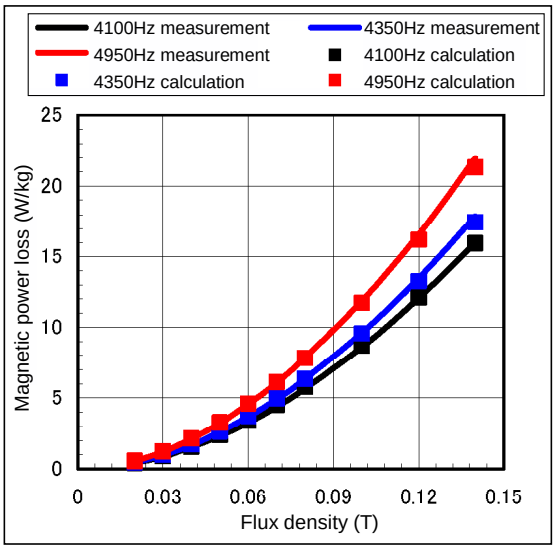

Fig. 1 Comparison between calculated values and measured values of magnetic power loss in single frequency mode

3. Calculation Method for Magnetic Power Loss by Fundamental Wave with Superimposed Harmonics[2]

The magnetic core of an actual motor has a flux waveform consisting of a fundamental wave and magnetic field with superimposed harmonics. For the purpose of this study, the magnetic power loss generated in actual motors is classified into five types as listed below:

(1) Fundamental wave hysteresis loss
(2) Fundamental wave eddy current loss
(3) Increment in fundamental wave hysteresis loss by harmonics
(4) Harmonic eddy current loss
(5) Minor loop hysteresis loss

The minor loop hysteresis loss[3] listed above is calculated from the flux density at a point where the minor loop is generated and the amplitude of the minor loop, as described in the references (3).

Figure 2 shows a comparison between the measured values and calculated values of magnetic power loss by fundamental wave with superimposed harmonics. It should be noted that the fundamental wave has a frequency of 100 Hz and the harmonics have a frequency of 2.5 and 5% of the fundamental. The figure clearly indicates sufficient accuracy of the calculation.

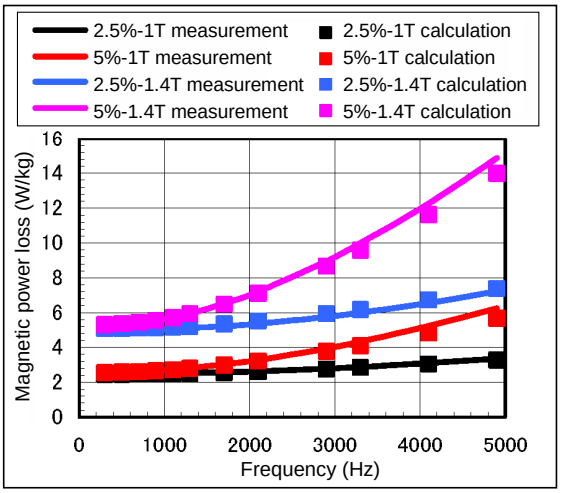

Fig. 2 Modeling of magnet power loss by fundamental wave with superimposed harmonics

4. Calculation of Deterioration in Magnetic Core

The magnetic properties and magnetic power loss characteristics of magnetic cores of rotating machines deteriorate through machining processes[4]. In this study, P-type deterioration (using coefficient *p*) and Q-type deterioration (using coefficient *q*) are considered in terms of deterioration of magnetic properties.

The flux density, $B_p(H)$, resulting from P-type deterioration is given by the following equation, with the original BH curve defined as $B(H)$:

$$B_p(H) = \mu_0(1-p)H + pB(H) \qquad (8)$$

where μ_0 is the magnetic permeability of a vacuum. The equation is based on the assumption that the magnetic core has non-elastic damage near the cut surface due to strain by core punching.

The magnetic flux, $H_q(B)$, resulting from Q-type deterioration, with the original BH curve defined as $H(B)$, is given below:

$$H_q(B) = \frac{(1-q)B}{\mu_0} + qH(B) \qquad (9)$$

This equation is based on the assumption that the deterioration is caused by residual stress in the compressive direction resulting from shrink fitting or the like.

Figure 3 shows a comparison between the measured values obtained when compressive stress (about 100 MPa) was applied and the calculated values of magnetic property considering magnetic core deterioration from the formulation above. The figure clearly indicates sufficient accuracy of the modeling.

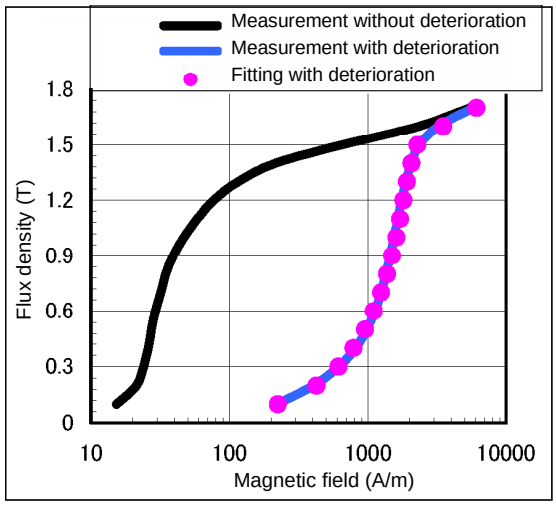

Fig. 3 Modeling of magnetic property considering magnetic core deterioration

For deterioration of magnetic power loss characteristics, coefficient u is calculated likewise. The hysteresis loss, W_h, after deterioration is given by the following equation:

$$W_h = \alpha B_u^{\gamma} fu \tag{10}$$

B_u is expressed by the following equation, using the magnetic property after deterioration, $H_r(B)$:

$$B_u = \frac{B - (1-u)\mu_0 H_r(B)}{u} \tag{11}$$

Figure 4 shows a comparison between the measured values obtained when compressive stress (100 MPa) was applied and the calculated values of magnetic power loss. The figure clearly indicates sufficient accuracy of the modeling.

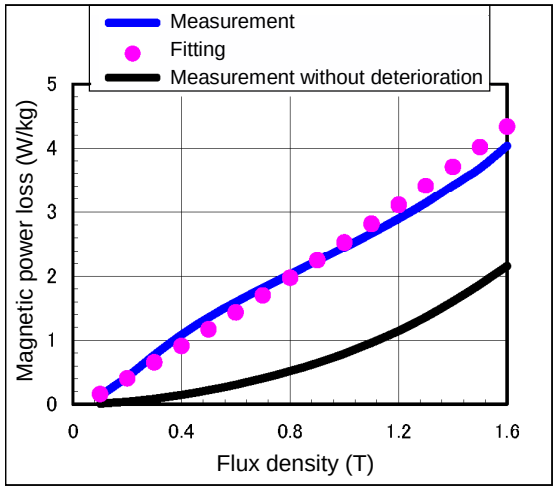

Fig. 4 Modeling of magnetic power Loss considering magnetic core deterioration

5. Analysis of Loss in Rotating Machines

The measured values of magnetic power loss represent losses other than copper loss under load, including the total mechanical loss and stray load loss in addition to loss occurring in the magnetic core. Stray load loss includes eddy current loss in rare earth magnets, at magnetic core edges, or frames, and additional copper loss due to the skin effect of coil winding subjected to high-frequency current.

Figure 5 shows a comparison between the measured values and calculated values of magnetic power loss analysis on the permanent magnet motor with the total losses mentioned above. The figure clearly indicates sufficient accuracy of the calculation.

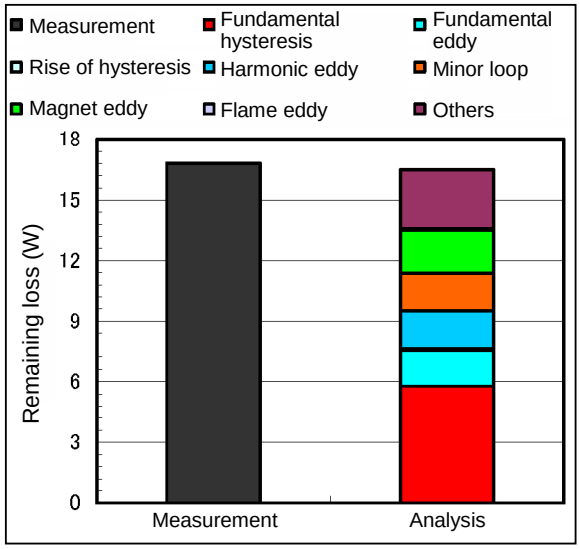

Fig. 5 Example of magnetic power loss analysis of permanent magnet motor

References

(1) IEEJ Technical Report No.1044: "Highly Accurate Modeling Technologies on Electromagnetic Analysis for Rotating Machines", (2006)

(2) H. Kometani and Y. Tani: "Analysis of Magnetic Power Loss Generated by the Flux Superimposed with the Harmonics", The papers of Joint Technical Meeting on Static Apparatus and Rotating Machinery, IEE Japan, RM-05-27, SA-05-27 (2005)

(3) Y. Tani and H. Kometani: "Influence on Core Loss Estimation in Distortion Wave by Approximation Method of Minor Hysteresis Loss (Continued Report II)", The papers of Technical Meeting on Magnetics, IEE Japan, MAG-05-44, pp.31 (2005)

(4) M. Nakano, A. Daikoku, S. Yamaguchi, Y. Tani, H. Arita, Y. Toide, T. Yoshioka and C. Fujino: "Cogging Torque Calculation Considering Distribution of Principal Stress of Stator Core in Permanent Magnet Motors", The papers of Joint Technical Meeting on Static Apparatus and Rotating Machinery, IEE Japan, RM-04-16, SA-04-16 (2004)

Multi-Domain Simulation of Drive Controls

Authors: *Kei Terada** and *Noriyuki Uchida**

Drive control units and their systems are characterized by different phenomena and technologies involving multi-domain physics across different technological domains. This report discusses multi-domain simulation effective in predicting multi-domain physics and effective measures for drive control units in the design phase.

1. Features of Drive Control Unit and Application of Multi-Domain Simulation

Drive control systems consisting of controllers, amplifiers, motors, etc. involve various phenomena and technologies that include control, mechanical, electrical, thermal, and electromagnetic factors and conditions. Moreover, research and development of drive control products requires optimum combinations of control, main circuit, motor, and machine components under respectively different conditions; design often requires a trade-off between technological domains.

Restrictive design requirements have recently increased along with advanced contents of user requirements and multi-domain physics involving several technological domains must be taken into consideration in many cases. In-depth knowledge about a single technological field may not work as an effective tool to solve today's problems.

Multi-domain simulation technology is expected to provide solutions for the technological problems we face today. Multi-domain simulation combines such aspects as electromagnetic field analysis, control system analysis, and thermal analysis to simulate phenomena of different technological domains simultaneously.

Use of multi-domain simulation will lead to prediction of multi-domain physics and application of effective measures for drive control units in the design phase to achieve a total optimum design across several technological domains, thus contributing to the realization of high performance and functionability of driving control units.

2. Control-Mechanical Coupling

Along with the recent trend toward lower weight and rigidity of machines as well as higher speed and accuracy of operation, vibration issues are gaining importance. Under such circumstances, mechanism design has become increasingly complex, including but not limited to, synchronous and/or collaborative driving systems using multi-axial configurations. As a result, simple mechanical models used for simulations in the past have become useless in many cases today.

Mitsubishi Electric employs coupled control-mechanical multi-domain simulation by extracting models from the results of modal analysis of machines using FEM and dynamics analysis using mechanism analysis tools (Fig. 1). This technology in particular serves the development of optimum control functions in machines, such as anti-vibration control in AC servo systems.

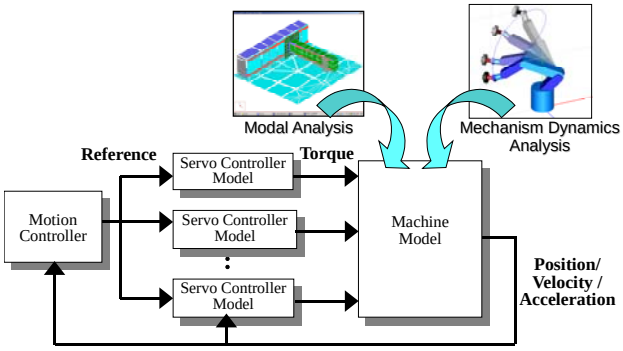

Fig.1 Controller-mechanical coupling simulation

Control system development at Mitsubishi Electric, in accordance with customers' machines, uses coupled control-kinematic simulation equipped with a 3-D visualization function, which makes it much easier to evaluate and examine total machine behavior of systems for complicated mechanical actions.

3. Electro-Thermal Coupling

Realizing thermal design of high cooling efficiency within a short period of time in the design phase, in response to increased iron loss in high-efficiency motors and increased copper loss resulting from higher output density, is indispensable for the reduction of development cost and improvement of quality.

In the field of electric design, improvements have been achieved in loss separation technologies and loss reduction technologies for the elements of motors under actual environmental and loading conditions.

By coupling these technologies with thermal design, quality enhancement by means of high-accuracy temperature prediction in the stage before trial manufacture

**Nagoya Works*

and examination of optimization of local thermal design have become possible. (Fig. 2)

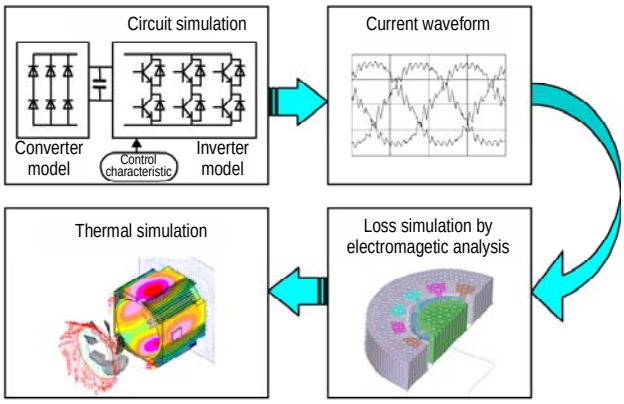

Fig.2 Electro-thermal simulation

Thermal design of the main circuit of the amplifier that drives the motor, another key item in drive control equipment, is also important. Higher heat-generation density of switching devices installed in the amplifiers has become increasingly common with the present trend toward switching devices of higher current and speed. Emphasis is placed on the importance of structural design with respect to thermal problems, such as optimization of equalized-heat arrangement of device parts, through the use of transient coupled electro-thermal simulation. (Fig. 3)

Real load and time series transient thermal simulation is possible by deriving device loss waveform under real load conditions by a circuit simulator and inputting the waveform in the thermal simulation.

4. Electromagnetic-Control Coupling

In this chapter, multi-domain simulation involving electromagnetic field and control is discussed.

The simulation aims at shortening the development time and reducing the cost by predicting phenomena generated as a result of mutual interference between the motor and amplifier in the design phase. Figure 4 shows the configuration of the multi-domain simulation. The calculation time is shortened by incorporating the highly accurate motor model obtained by the electromagnetic field analysis.

The calculation results for an interior permanent magnet motor were compared with the measured results. The motor model includes the nonlinear magnetization property of the material, rotor-position dependency of the magnet flux, current and rotor-position dependency of inductance and torque. The motor control is vector control using sensors, with a constant speed and no field weakening for both simulation and measurement.

Figure 5 shows the measured results and coupled simulation results of current waveforms under a fixed load and at a fixed operation speed.

This figure plainly shows that the pattern of influence of the carrier frequency and the trend of current waveform distortion near the peak point and zero point agree well with the actual system.

5. Real-Time Simulator for Power Electronics

The newly developed real-time simulator for power electronics can reproduce phenomena on the order of microseconds by switching the power device.

Here, we present HILS (hardware-in-the-loop simulation) based on the real-time simulator [1] (Fig. 6).

HILS can accurately reproduce current distortion at

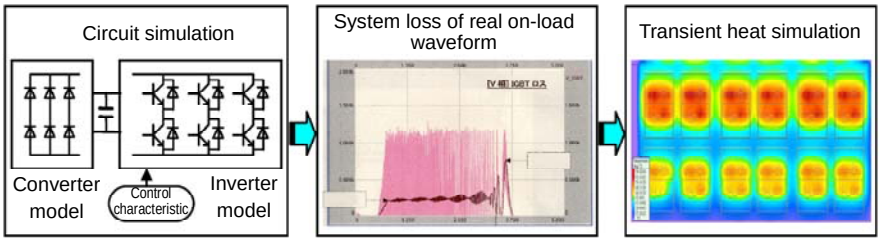

Fig.3 Transient heat simulation of amplifier

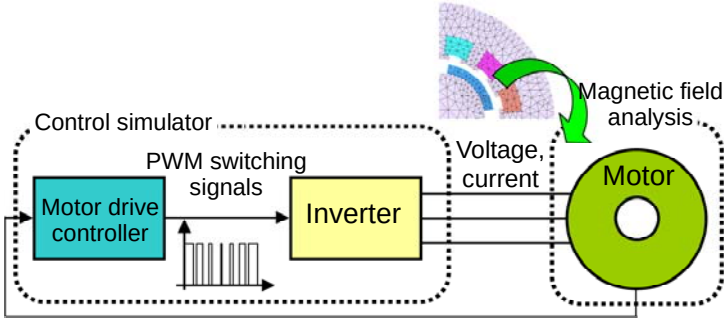

Fig.4 Modeling and combine to control simulation

a dead time, Td, shorter than the calculation time, 10 µsec, as a result of optimizing the FPGA I/O board having long-time resolution as well as the model (Fig. 7). HILS is an extremely useful method; it does not require an actual inverter or motor and it can perform various types of verification involving operating conditions that cannot be easily employed in an actual system.

6. Conclusion

Mitsubishi Electric will make every effort to further improve multi-domain simulation technologies for application to the development of drive control equipment. We will continuously, and quickly, provide products that satisfy the needs of the users.

Reference

(1) Masaya Harakawa, et al.: Real-Time Simulation of a Complete PMSM Drive at 10 µs Time Step, IPEC Niigata 2005, S27 (2005)

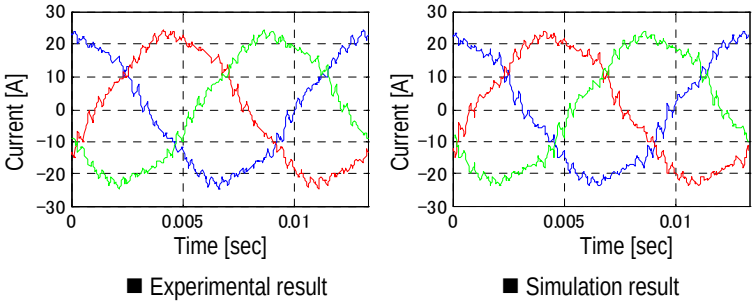

Fig.5 Comparison of experiment and simulation result

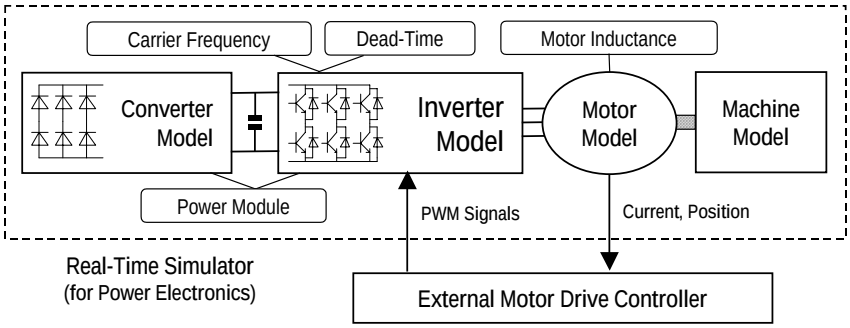

Fig. 6 HIL simulation of the motor drive

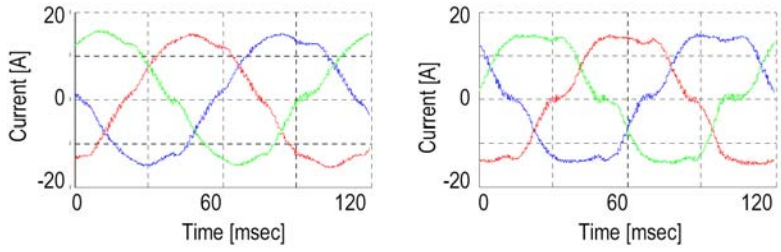

(a) Td = 4.2 [µsec] (b) Td = 12.8 [µsec]

Fig. 7 HIL simulation result (effect of dead-time)

Electromagnetic Driving Technology of DC Motor for EGR Valve

Authors: *Youichi Fujita** and *Moriyuki Hazeyama***

With worldwide reinforcement of regulations on automobile exhaust gas, the market demand for exhaust gas recirculation valves (EGR valves) has grown rapidly. In response, Mitsubishi Electric developed a DC motor-driven EGR valve for diesel engine applications. This paper introduces a further modified EGR valve designed to meet the needs of automobile makers in terms of the electromagnetic structure of motors and, at the same time, to meet the structural specifications of Mitsubishi Electric's EGR valves.

1. DC Motor-Driven EGR Valve for Diesel Engines

EGR valves for diesel engines must provide high flow-rate control, high-speed response, high-precision control, and a self-return function (the valve must be closed only by spring force). With these performance aspects taken into consideration, we developed and employed a DC motor compact in size and able to generate high torque.

The DC motor basically employs a brushless structure with a magnetic rotating mechanism. It obtains brush motor characteristics by incorporating a commutator and slip ring for mechanical commutation and power distribution (Fig. 1(a)). It features high-response performance resulting from low inertial of the rotating element, direct-acting thrust obtained by the screw-type rotation / direct action conversion mechanism provided inside the magnet rotating section, self-returning operation, and positional stability against external force working on the valve.

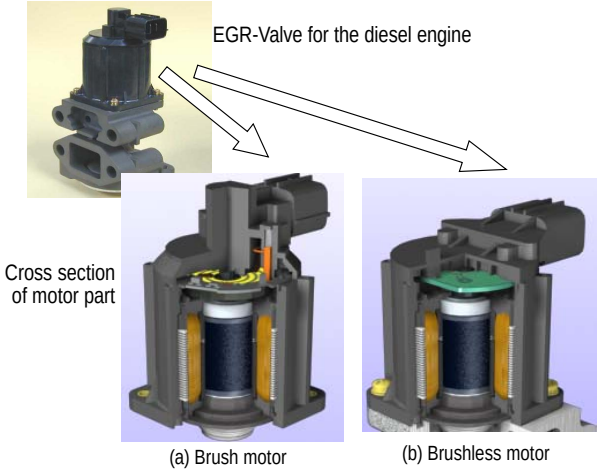

Fig. 1 EGR-Valve for the diesel engine

The coil winding section of the motor employs Mitsubishi Electric's original "Poki-Poki" core structure (Fig. 2), contributing to the realization of highly efficient and productive motors. Additionally, the brushless motors have the merit of being manufactured on the same production line as brush motors, as they are basically of the same structure.

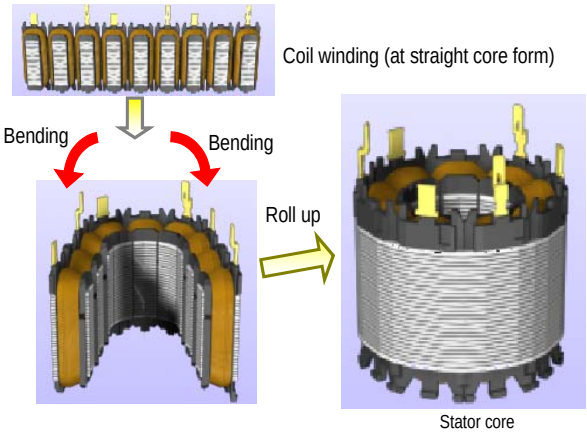

Fig. 2 Composition of "Poki-Poki" core

2. Design Requirements

According to a comparison between Mitsubishi Electric and another manufacturers on the thrust of DC motors for EGR of the same dimensions (Table 1), Mitsubishi Electric's DC motor features higher motor output than the others for the same level of thrust, which confirms it as a high-torque product. Furthermore, with its low reduction ratio, the rotational speed of the motor before reaching the target aperture of the valve is also low. In other words, the design requirements of Mitsubishi Electric's DC motor for EGR valves are high torque and low rotational speed.

Table 1 Output power of DC motor for EGR-valve

Motor	Motor output	Reduction system	Thrust
DC motor of other make	1/3	Gear-reduction Cam-reduction x3	1
Mitsubishi DC motor	1	Screw-reduction x1	1

*Sanda Works **Advanced Technology R&D Center

3. Electric Design for Higher Torque

Higher torque requires an increase in magnetic flux or ampere turn. In this DC motor, a polar anisotropy magnet is employed to increase magnetic flux for higher torque. In addition, for increased torque without changing the current level, the number of coil turns and the teeth width are optimized in the design stage based on analysis.

For increased flux, which is essential for developing torque, it is important to reduce the leakage flux. This DC motor employs the optimum design for slot openings and teeth tips to minimize torque reduction and leakage flux at the same time.

4. Design of V-Notch for Stator Core

To secure motor torque as required, the relationship between the width of the connecting section and the gap created in the V-notch butting point (Fig. 3) must be carefully considered. We examine the relationship by using the magnetic field analysis described below.

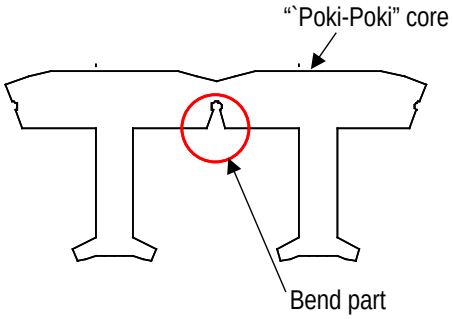

Fig. 3 Bend part of "Poki-Poki" core

If the gap in the V-notch butting point is large, the magnetic flux concentrates on the thin connection section, increasing the magnetic flux density therein and resulting in a magnetic flux leak, as shown in Fig. 4 for the analysis results on magnetic flux density distribution. In short, the gap in the V-notch butting point is responsible for reduced torque output.

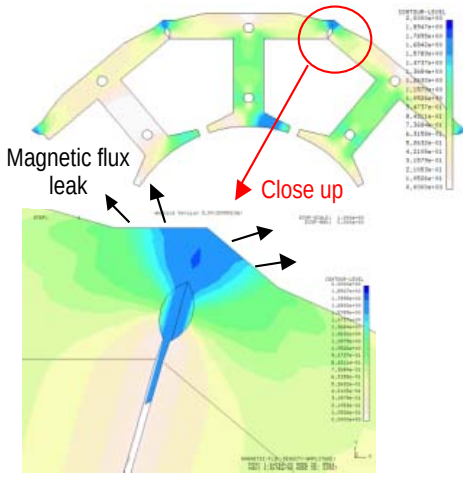

Fig. 4 Distribution of magnetic flux density at the tin bending part of core (large gap)

In this DC motor, the stator core is pressurized inward from the periphery by integral molding of resin, which has the structural advantage of reducing the gap in the V-notch butting point. Figure 5 shows the results of magnetic flux density analysis with a small gap in the V-notch butting point. Compared with the results shown in Fig. 4, the magnetic flux density in the thin connecting section is lower in Fig. 5, which indicates that the magnetic flux leak is reduced. With the magnetic flux leak reduced as described above, high torque is achieved.

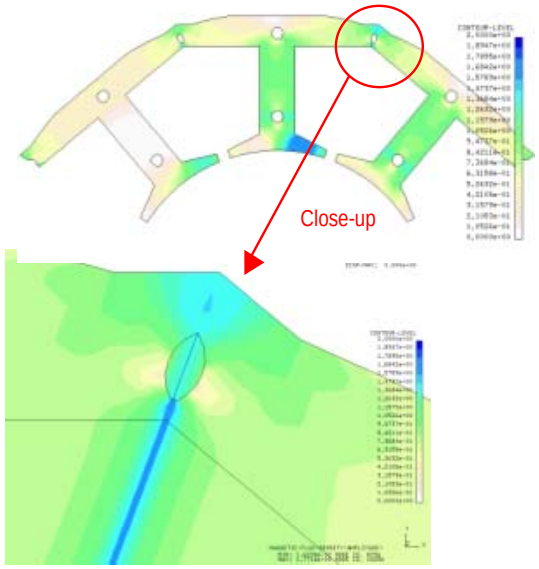

Fig. 5 Distribution of magnetic flux density at the thin bending part of core (small gap)

5. Number of Magnetic Poles and Stator Core Slots

Besides reducing the gap in the V-notch butting point, magnetic flux leak can be reduced by employing multi-pole magnets. However, the number of magnetic poles and stator core slots has an upper limit due to restricted configuration involving rotors and stators.

Mitsubishi Electric's EGR valves must be able to perform self-return valve operation, which makes it necessary to suppress torque ripples (cogging torque) while the valve is not energized. As a measure against toque ripples, a combination number of magnetic poles and stator core slots can be taken into consideration. In view of optimizing the V-notch configuration in the stator core and the shape of the teeth as mentioned above, we selected 8 poles and 9 slots. We confirmed through analysis that the size of the cogging torque is sufficient and reasonable for normal self-return operation.

6. Cost Reduction through Electromagnetic Design

Motor loss is largely classified into two types: copper loss generated in the stator winding and iron loss generated in the stator core. High-density winding is

realized by using concentrated winding with the Poki-Poki core, resulting in successful reduction of copper loss.

Iron loss largely depends on the rotational speed of the motor. This DC motor, which is not intended for continuous rotation, operates at a low rotational speed with limited iron loss that can generally be ignored. This means that the electromagnetic steel sheet used for the stator core may be of low grade.

7. Conclusion

Exhaust gas regulations and fuel efficiency standards will become even stricter in the future and the demand for improved performance in terms of output, response, and durability will grow accordingly. To meet these needs and develop products with revolutionary market performance, we intend to make the best use of effective development tools such as magnetic field analysis to identify our own technological weak points at an early stage and to shorten the time required for experimental manufacture, to achieve our target of producing compact and highly efficient motors with low mechanical and electrical loss.

Electromagnetically Actuated Vacuum Circuit Breaker

Authors: *Masahiro Arioka** and *Tae Hyun Kim***

Mitsubishi Electric Corporation has commercialized a 12/24-kV electromagnetically actuated vacuum circuit breaker that employs double-yoked advanced bi-stable electromagnetic actuators designed to perform both opening and closing operations linearly by means of electromagnetic force and maintain its open or closed state with the help of the magnetic force of permanent magnets. By adopting an electromagnetic actuation method for the vacuum circuit breaker, we have eliminated the need for parts that can wear out, halved the number of parts, significantly enhanced reliability and obviated the need for maintenance of the actuators.

1. Introduction

Mitsubishi Electric Corporation has implemented a 12/24-kV electromagnetically actuated vacuum circuit breaker (hereinafter referred to as VCB) that employs double-yoked advanced bi-stable electromagnetic actuators designed to perform both opening and closing operations by means of electromagnetic force and maintain its open or closed state with the help of the magnetic force of permanent magnets. We have eliminated parts such as latching levers which are susceptible to wear by employing electromagnetic actuators which directly actuate (in a direct-acting manner) the main contacts in a straight line and also halved the number of parts by avoiding the intermediate linkage arrangement. As a result, along with significantly increased reliability, we have reduced the life-cycle cost by obviating the need for maintenance of the actuators.

In VCB development in the past, there was no method for conducting sophisticated analysis of the actuation characteristics of VCBs, each of which consists of multiple mechanical parts such as contact-containing vacuum interrupters, insulating rods, contact pressure springs, and electromagnetic actuators, so it was difficult to reduce the amount of energy required to open/close VCBs. We have therefore newly developed and applied a technology called "electromagnetic analysis coupled with motion" which faithfully simulates the construction of VCBs. Using this technique, we have optimized the construction and created one of the world's highest-efficiency electromagnetically actuated VCBs, reducing the actuation energy by 80% compared with conventional VCBs.

2. Overview of the Electromagnetically Actuated VCB

Table I shows the distinguishing features of the electromagnetically actuated VCB. Compared with our conventional VCBs (spring-loaded type), the number of parts has been decreased to 45%. This has enhanced reliability, while the elimination of wear-susceptible parts and the need for greasing means that maintenance is no longer necessary. In addition, we have adopted an actuation method in which vacuum interrupters, insulating rods, contact pressure springs, and electromagnetic actuators are arranged in line with one another so that the actuators for the three phases are operated by only one shaft, thus eliminating the three-phase link arrangement.

Table 1 Features of electromagnetically actuated VCB

Concept		Features
Environmentally friendly		• Reduces the driving noise
Reduction of life cycle costs	Operation	• Reduces the required operation energy
	Maintenance	• Not require maintenance for over 15 years • Application of anti-oxidation grease
Safe design High reliability		• Simple structure • Minimum parts number • Directly and straight operation • No wear parts (80,000 times CO operation have been confirmed)

Table 2 shows the ratings and specifications whereas Fig. 1 shows a representative VCB construction. Figure 2 shows the electromagnetic actuator construction which is simple in design, consisting of the first fixed yoke, the second fixed yoke, the permanent magnet, the plunger and the closing/opening coil. The permanent magnet makes it possible to hold either the open or closed state without external energy. Opening or closing operation is performed by applying electric energy stored in a capacitor to the opening or closing coil by means of control circuitry. The second yoke construction is unique to our company. Figure 3 shows the principle of operation. As shown in Figs. 3 (a) and (b), by making the permanent magnet's magnetic path (for opening/closing-pole retention) and the coil-excited magnetic path (for opening/closing action) as separate entities, it is possible to enhance the efficiency of opening/closing (make/break) action without causing counter-magnetization of the permanent magnet. Moreover, we have made the plungers using a lami-

*Power Distribution Systems Center **Advanced Technology R&D Center

nated construction in order to minimize eddy current during driving, and thus save energy.

Table 2 Ratings of electromagnetically actuated VCB

Item			Rating	
Rated voltage		(kV)	12	24
Rated withstand voltage	BIL	(kV peak)	75	125
	AC	(kV rms)	28	50
Rated frequency		(Hz)	50 / 60	
Rated normal current		(A)	630, 1250	
Rated short-circuit breaking current		(kA)	25	
Rated short-circuit making current		(kA)	63	
Rated short-circuit withstand current		(kA)	25 (3 sec)	
Break time		(cycle)	3	
Standard			IEC, JEC	

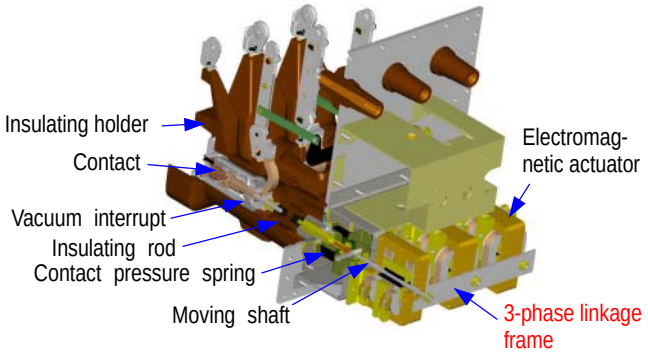

Fig. 1 Structure of electromagnetically actuated VCB

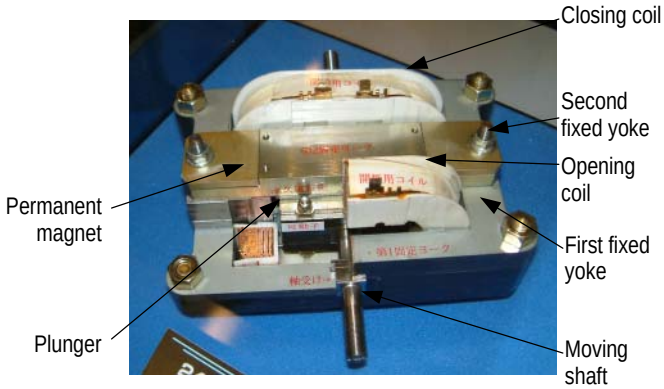

Fig. 2 Cut model of electromagnetic actuator

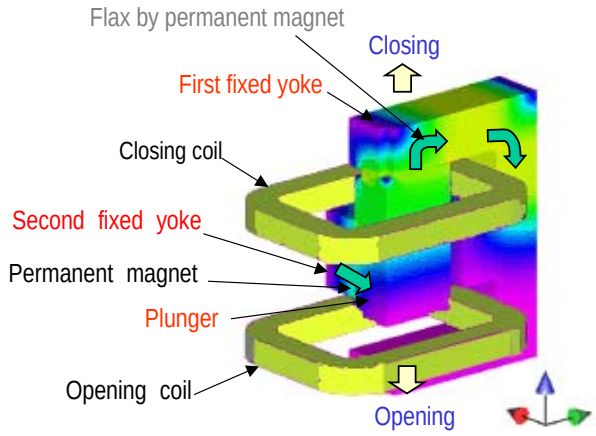

Fig. 3 (a) Contact closed

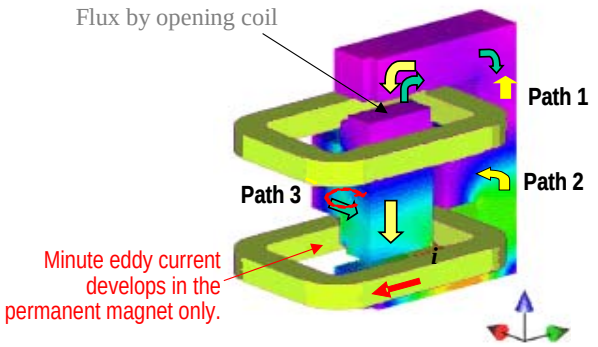

Fig. 3 (b) Open working

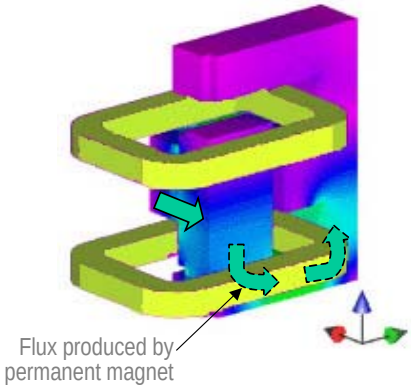

Fig. 3 (c) Contact opened

3. Coupled-Analysis Technology

In the case of the "electromagnetic analysis coupled with motion" technique, the locational dependency of magnetic flux that is generated in the vicinity of the plunger of each electromagnetic actuator, electromagnetic force-producing coil current, and the plunger is determined by means of 3-D FEM static electromagnetic analysis and Equations (1-1), (1-2) and (2) are analyzed in a coupled manner.

$$\frac{q(t)}{C} + I_{coil}(t)\cdot(R_{coil}+R_{out}) + \frac{d\phi(I_{coil}(t),z(t))}{dt} = E \quad \cdots\cdots \text{(1-1)}$$

$$\frac{dq(t)}{dt} = I_{coil} \quad \cdots\cdots\cdots\cdots\cdots\cdots \text{(1-2)}$$

$$m(z(t))\frac{d^2z}{dt^2} = Fm(I_{coil}(t), z(t)) + Fs(z(t)) + F_{friction} \quad \cdots \text{(2)}$$

The delay of magnetic flux and electromagnetic force due to eddy current was expressed using a time constant τ and was incorporated into the magnetic flux (ϕ) and electromagnetic force (F). The time constant τ was determined based on the results of an actuation test run on the electromagnetic actuator alone. Furthermore, discontinuity in changes in the mass of the circuit breaker's moving section was considered by applying the law of conservation of momentum. Figure 4 shows the results of the above-mentioned analysis (plotted by open circles) and the results of actual

measurements (solid line), both conducted upon opening of the VCB. The upper graph shows time-varying changes in opening stroke while the lower graph shows time-varying changes in coil current. By applying the time constant τ and the law of conservation of momentum, the analytical results agreed well with the measurement results for both stroke and coil current. Thus, it is possible to precisely reproduce the opening/closing characteristics of the electromagnetic actuators using the above-mentioned analytical method. We developed an optimum design using the analytical method, resulting in an 80% reduction of the required actuation energy compared with conventional spring-loaded actuators. Using the analytical method, we have also studied variations in opening and closing times caused by the manufacturing and assembling tolerances of parts (see Table 3). As shown in the table, the variations in opening and closing times were extremely small, typically within 0.5 ms as measured on our prototypes.

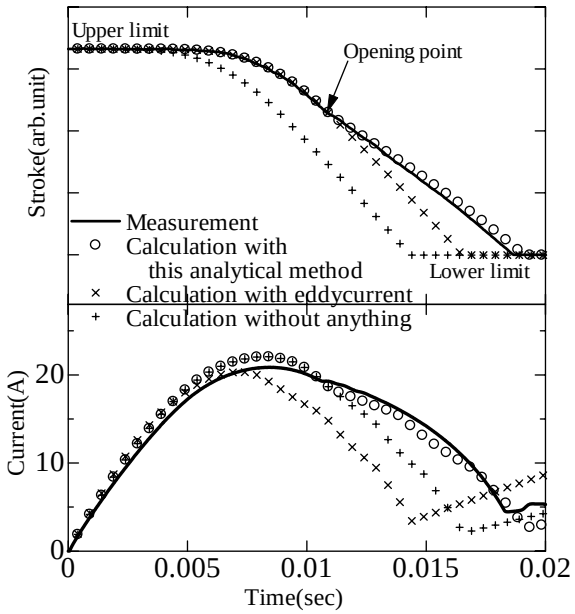

Fig. 4 Calculated and measured strokes and currents on the opening operation

Table 3 The calculated time difference of the driving behavior among three phases

	Worst (100%)	3σ (99%)	2σ (95%)
Opening time difference (ms)	2.8	2.0	1.3
Closing time difference(ms)	3.4	2.4	1.6

4. Summary

The 12/24-kV electromagnetically actuated VCB introduced in this paper has been in operation at power receiving and distribution facilities since 2004. We plan to roll out the electromagnetically actuated VCB to other ratings and thereby integrate them into a product series.

FR-A700 Series Next-Generation High-Functionality General-Purpose Inverters

Authors: *Katsushi Ikeda** and *Yasuhiro Shiraishi**

Over the past several years, significant advances have been made in inverter control as a means of driving motors. In the field of general-purpose inverters for use in conveyor/transport systems, lifting/hoisting equipment, machine tools, etc., the market sought high-performance and easy-to-use inverters capable of addressing a broad range of operating conditions such as drive performance at low speeds, maintainability, maneuverability, environmental resistance, and remote parameter setting as well as accommodating a wide variety of uses.

The improvements in drive performance include enhanced precision of "Offline auto tuning without motor running," a feature that was first adopted in the FR-A500/A500L series to estimate motor constants, and the incorporation of "Real sensorless vector control," which was developed by making considerable improvements over the conventional advanced magnetic flux vector control in terms of speed control range and velocity response. What is more, through the addition of a built-in PLG (Pulse Logic Generator) input interface option, "Vector control with PLG" has become possible. As a result, not only highly-responsive speed control but also torque control and positional control can be accomplished.

We have also successfully incorporated the following, all of which made their way into earlier "FR-F700 Series" full-fledged inverters for fan- and pump-drive applications and have been well-received in the marketplace: "Enhanced maintainability," "Improved maneuverability," "Incorporation of an EMC filter," and "Support for a wide variety of networks".

Enhanced drive performance	Real sensorless vector control and vector control with PLG are incorporated.
Easy maneuverability	New FR-PU07 parameter unit lineup
	Easy setup made possible by USB connection
Excellent expandability	Support for networks (CC-Link Ver. 1.1/2.0), CANopen, Ethernet, SSCNET III, etc.) Brake transistors rated at 22 kW or smaller can be incorporated. With the addition of options, serious vector control becomes possible.

Fig. 1 Next generation high performance inverter "FR-A700 series"

**Nagoya Works*

1. Product Overview

The FR-A700 series product overview is shown in Table 1. The series lineup features 200V and 400V versions in as many as 17 capacities ranging from 0.4 to 90 kW and 29 capacities ranging from 0.4 to 500 kW, respectively.

Since the FR-A700 series is equipped with functions suited to speed-varying applications such as real sensorless vector control, for conveyor/transport systems, lifting/hoisting equipment, machine tools, etc. as well as fit for line-control applications for winders, printing machines, etc., it offers expandability to support serious vector control and a wide variety of networks via the addition of options.

Table 1 Overview of FR-A700 Series Inverter Specifications

No.	Item		FR-A700 series inverter specifications
1	Voltage and capacity		0.4 to 90 kW at 200V (Provision for 240V can be made.) 0.4 to 500 kW at 400V (Provision for 480V can be made.)
2	Output frequency range		0.2 to 400 Hz
3	Control methods		High-carrier-freq. PWM control Advanced magnetic flux vector control Real sensorless vector control Vector control with PLG (when the optional FR-A7AP is used)
4	Major functions	For use with conveyor/ transport systems and lifting/ hoisting equipment	Multi-speed operation, bumping-stop selection, brake sequence, droop control, offline tuning, machine analyzer, easy gain tuning, velocity feed forward, DC power input, pulse train input/output
		Maneuverability and maintainability	Life diagnostic function, maintenance timer, current average value monitor signal, simple mode, cooling fan ON/OFF control
5	Communication	Standard equipment	RS485 and Modbus-RTU
		Options	CC-Link, LonWorks, DeviceNet, Profibus-DP, Ethernet and CANopen
6	Construction	Protective construction	IP20 (22 K or less)
		Brake	Brake transistor: 22 K or less incorporated Brake resistor: 7.5 K or less incorporated
		Control terminal block	Removable (A500 series control terminal block can also be connected.)
		Cooling fan	Available in easy-to-replace cassette form (for all capacities)
		DCL	Connectable for all capacities
7	Supported standards		UL, cUL, EN Standards, EMC: 2nd Environment (EMC filter incorporated)

2. In Pursuit of Further Enhanced Drive Performance

2.1 Enhanced precision of offline auto tuning without motor running

Beginning with the earlier "FR-A500/A500L Series," we introduced an offline auto tuning function for drive motors whose electrical constants are unknown under advanced magnetic flux vector control.

There are two modes for offline auto tuning: one in which the motor is running, and the other in which the motor is at a standstill (hereinafter referred to as offline tuning). Both methods are intended to estimate the electrical constants of the motor as shown in Fig. 2. Conventionally, in the online mode (that is, tuning with the motor running), the self inductances L1 (= M + λ1) and L2 (= M + λ2) can be easily estimated. However, in the case of offline tuning, it has been difficult to obtain a sufficient degree of precision.

For the "FR-A700 Series," we made provision to enable high-precision tuning of self inductances L1 and L2 without having to rotate the motor, making it possible to achieve favorable drive under advanced magnetic flux vector control or real sensorless vector control under conditions where it is difficult to actually rotate the motor – for example, where already-existing facilities are involved.

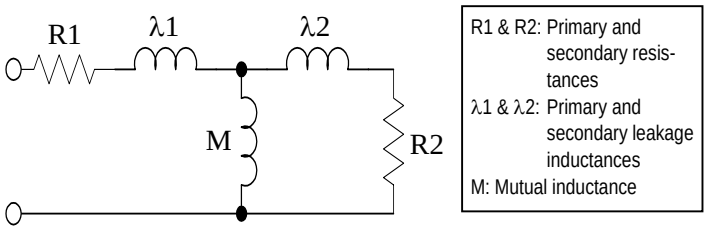

Fig. 2 T-Type equivalent circuit of motor

2.2 Real sensorless vector control

As opposed to the conventional advanced magnetic flux vector control, we configured a vector control system without rotational speed detector and incorporated real sensorless vector control that realizes high-precision speed control and torque control. In this control scheme, we configured an adaptive magnetic flux observer to accurately calculate/estimate magnetic fluxes from voltage and current. Figure 3 shows its block diagram.

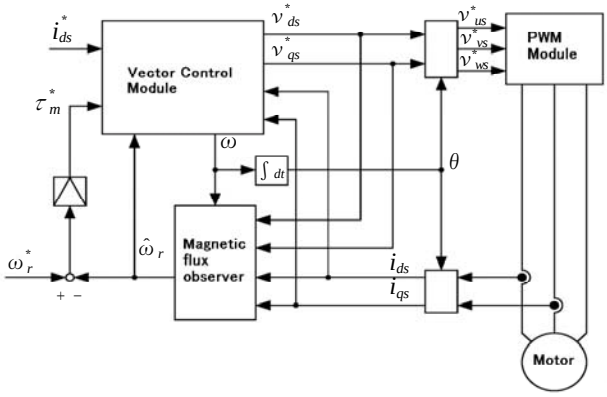

Fig. 3 Block diagram of real sensorless vector control

Unlike conventional vector control where calculations are made using actual speed as determined by a

rotational speed detector such as a PLG, vector control calculation is performed using velocity estimated from magnetic flux as obtained from the above-mentioned flux observer in the case of the real sensorless vector control. Furthermore, under this control scheme, sensorless vector control featuring excellent stability is made possible through the use of the electric motor constants as determined by the aforementioned offline auto tuning.

2.3 Vector control with PLG

Even with the earlier "FR-A500/A500L Series," vector control was possible through the addition of the FR-A5AP option. However, this provision applied to speed control only.

In the case of the new "FR-A700 Series," high-precision vector control with PLG has been achieved on a par with our "FR-V500/V500L Series" vector inverters in terms of torque control, position control, etc. through the addition of the FR-A7AP option.

Table 2 compares the performance of the "advanced magnetic flux vector control," "real sensorless vector control" and "vector control with PLG," all of which are incorporated in the "FR-A700 Series" inverters.

By virtue of incorporating these varied control schemes, the ability to provide solutions for almost all conceivable uses has become a reality.

Table 2 Performance comparison of control schemes

	Advanced magnetic flux vector control	Real sensorless vector control	Vector control with PLG
Speed control	○	○	○
Torque control	×	○	○
Position control	×	×	○
Speed control range	1:120	1:200	1:1500
Velocity response	20 to 30rad/s	120rad/s	300rad/s

2.4 Easy gain tuning

When it comes to vector control with PLG, since it is necessary to adjust control parameters such as speed control gain in keeping with the characteristics of load machinery, the advent of auto tuning capability for control parameters has long been anticipated.

In the new "FR-A700 Series," we incorporated an easy gain-tuning function that estimates the load inertia on the fly with high precision under actual operating conditions and, thereby, automatically adjusts the velocity gain. This provision makes it possible to achieve high-precision speed control without the need for adjustment.

Figure 4 shows a waveform observed in the course of easy gain tuning. As can be seen from this figure, the inertia assumption value converges toward the true value with each acceleration/deceleration, meaning that speed control is automatically adjusted and the overshoots in the velocity waveform gradually diminish.

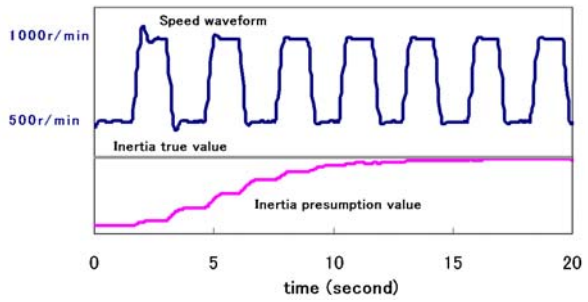

Fig. 4 Waveform of easy gain tuning operation

Since a USB interface (Ver.1.1) is provided as standard, it has become possible to easily perform setup and parameter management (such as parameter setting, file saving and printing) from a personal computer using software dubbed FR-Configurator.

What is more, the user can remove the FR-DU07 control panel from the inverter surface and connect the optional FR-PU07 parameter unit instead. Equipped with an LCD screen that is easy to see and a ten-key pad that allows direct entry, the FR-PU07 facilitates the setting of parameters and operation of the motor. Moreover, the use of the FR-PU07BB with its built-in battery allows the user to set and copy parameters without the need to turn on the inverter.

As for network support, an RS485 terminal block is provided as standard, and Mitsubishi inverter's proprietary protocol and Modbus-RTU protocol communications are supported as standard. In addition, we have made provision to support varied open networks such as CC-Link, LonWorks, DeviceNet, Profibus-DP and CANopen by means of options.

3. Conclusion

In this report, we introduced the FREQROL-A700 Series products designed to serve as high-functionality general-purpose inverters for applications such as conveyor/transport systems, lifting/hoisting equipment, machine tools, printing presses, etc. In view of future requirements for enhanced drive performance, environmental resistance and ease of use, we are determined to further step up our research and development efforts.

References:

(1) A. Satake, T. Kaitani: "Leading-Edge Motor Control Technologies" ADVANCE Sep.2003/Vol.103

(2) Y. Shiraishi, K. Ikeda: "Next-generation Energy-saving Inverter "FR-F700 series" ADVANCE Dec. 2005/Vol.112

Driving system MDS-D/DH series for M700

Authors: *Toshiki Tanaka** and *Kazuhiko Tsutsui**

In the field of machine tools, there is heightened demand not only for increased feed shaft speed and precision but also for enhanced spindle performance and functionality, all of which combine to influence the performance of the machine tool. Given this situation, among the constituent components making up NC systems, the drive unit plays an increasingly important role. To address the latest requirements, we developed and commercialized the MDS-D/DH series (servo/spindle drive units) to serve as M700 series CNC-ready drive systems. This system significantly boosts the productivity of machine tools thanks to the technologies described below.

1. Overview of the MDS-D/DH Series

Figure 1 shows the basic configuration of an M700 series CNC-ready drive system. For use as servo/spindle drive units, we provide 200V- and 400V-rated units, series MDS-D and MDS-DH, respectively. As for networking between NCs and servomotors, a high-speed optical network is adopted for high-speed transmission and reception of nano-order positional information and high-speed communication among drive units.

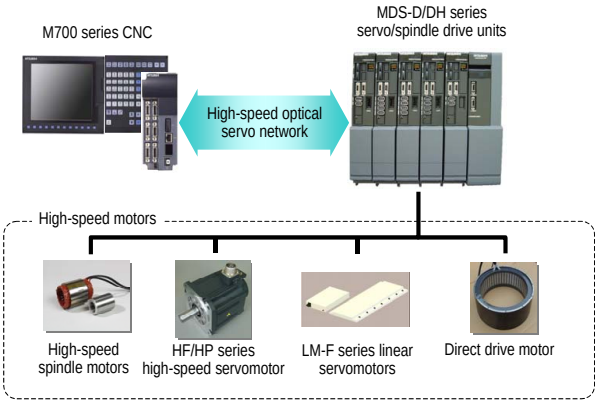

Fig. 1 Drive system of M700 series

2. Speed- and Precision-Enhancing Technologies

2.1 Enhancement of speed and torque

In the M700 series drive system, a combination of (HF/HP series) high-speed servomotors featuring significantly improved magnetic and electrical motor characteristics and (MDS-D/DH series) servo drive units equipped with a control scheme designed to deliver the best possible characteristics in those motors, achieves increased speed and torque, thereby enhancing machine productivity. Figure 2 shows this system's torque characteristics and confirms the achievement of characteristics that prevent torque from decreasing at higher speeds than before and thereby maintain high torque into the high rev range.

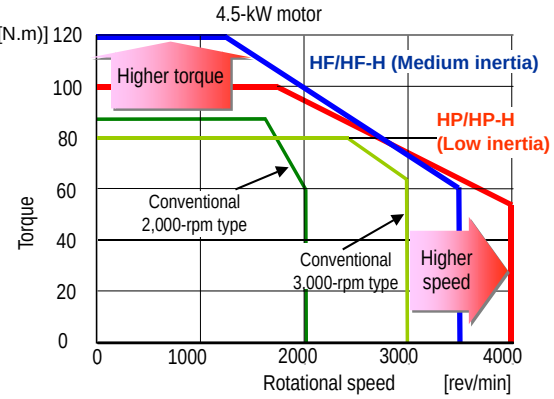

Fig. 2 Torque characteristic

2.2 Improvement of Basic Performance

The enhancement of control-loop responsivity (or high gain) is a basic requirement for improving machine speed and precision. To do this, we needed to increase the PWM frequency in order to shorten the time wasted in the control loop. However, raising the PWM frequency increases heat generation caused by switching loss, which constrains unit downsizing and energy savings. We therefore developed our proprietary current control technology and incorporated high-responsivity current control that minimizes the required PWM frequency increase while enhancing control stability.

In addition, we increased the resolution for positional and velocity feedback (to 1.6 million pulses/rev. for servo (optional) and 4 million pulses/rev. for spindle (when the number of detector teeth is 128)). Moreover, we enhanced total drive-system performance through combination with (HF/HP series) high-speed high-precision servomotors that have cogging torques as low as one third of those for conventional servomotors. Figure 3 shows the deviation from circular form as measured during circular operation under two-axis servo control. Compared with a conventional series, an

*Nagoya Works

approximately 5-fold increase in roundness was achieved thanks to the use of MDS-D/DH and HF series servomotors.

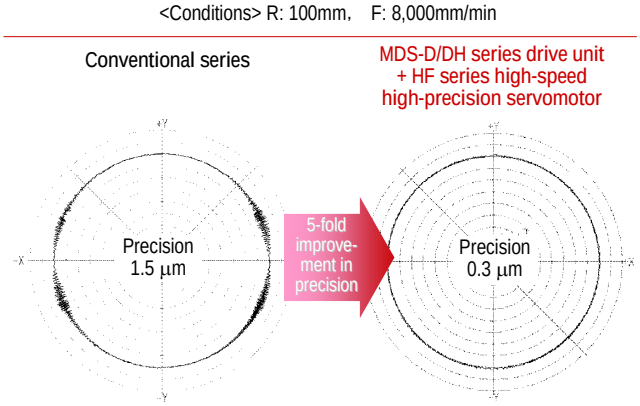

Fig. 3 Effectiveness of servo basis performance improvement (Comparison of circle accuracy)

Figure 4 shows heat generation in a spindle motor running at 12,000 rpm. It can be seen that the improved basic performance of the spindle (under high-responsivity current control) significantly decreased the harmonics of the current, thus reducing the heat generation caused by iron loss in the motor.

2.3 Spindle Servo Technology

In the case of conventional spindle driving, it was necessary to switch the control loop from speed control to positional control when shifting from a mode in which the spindle was simply rotated at high speed to a mode that required interpolation control with a servo arrangement such as the C-axis or a synchronization tap. As a result, every function changeover required an action such as return-to-origin operation, which hindered reductions in machining times. The reason why the spindle could not be operated under positional loop control at all times was that it was necessary to operate not only in a low-torque region but also in a low-output or torque saturation region, and there was a possibility of inducing overshoots and oscillation under a permanent position command due to torque saturation.

In response to the requirement for spindle control of the MDS-D/DH series, we used the follow-up delay compensation control as shown in Fig. 5 and achieved the capability to follow spindle-end-position-related commands from the NC by suppressing the effects of torque saturation (such as overshoots and oscillation) at the time of acceleration/deceleration, which used to be a challenge of permanent positional loop control. This has made it possible to configure a permanent position loop, thus eliminating the need for spindle-to-C-axis switchover that was required in the past, reducing the need for post-gear-change return-to-origin operation and greatly reducing processing times.

2.4 OMR (Optimum Machine Response) Control

To achieve optimum machine responsivity, we have developed the OMR-DDC (Direct Detect Compensation) control function. In the case of the M700

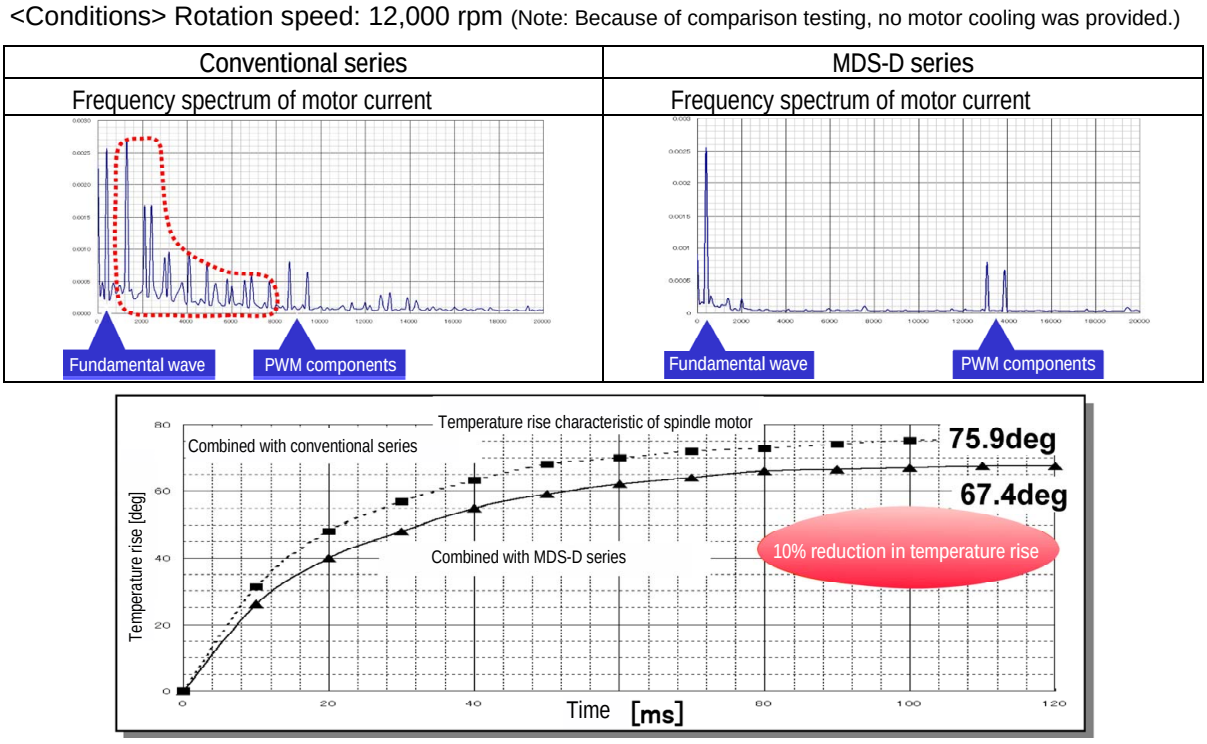

Fig. 4 Effectiveness of spindle basic performance improvement (Comparison of motor temperature)

series, we increased the communication rate by a factor of 10 and the communication period by a factor of 8 compared to the previous values with a high-speed optical network. This high-speed communication made it possible to achieve the OMR-DDC function, which enables information to be shared among drive units and data to be used for feedback control.

Figure 6 shows an example application of the servo-spindle inter-drive-unit compensation (OMR-DDC function) when a synchronization tap is used by means of the aforementioned spindle servo technology. This suppresses the increase of synchronization error due to the saturation of spindle torque and shortens of time constants.

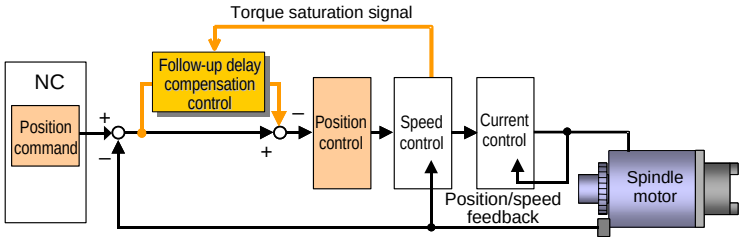

Fig. 5 Spindle control of MDS-D/DH series

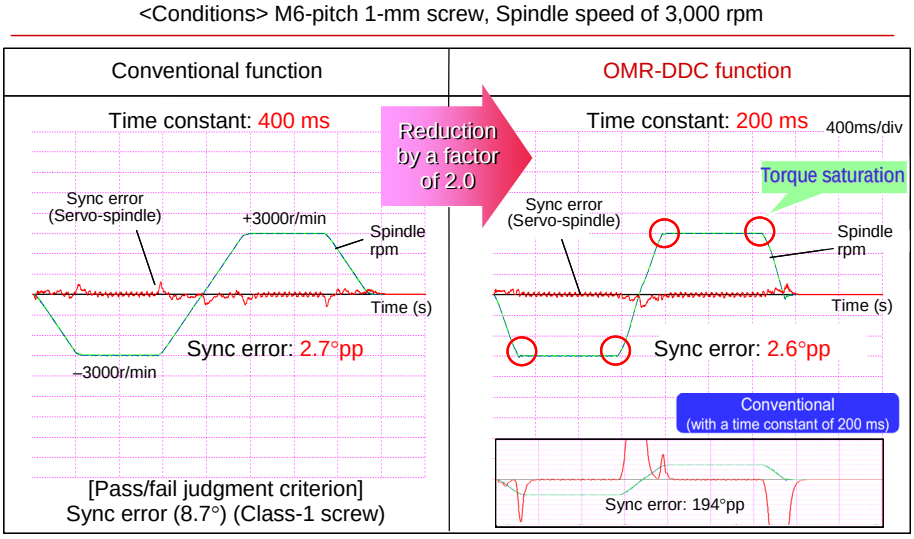

Fig 6 Synchronization tap time shortage by OMR-DDC function

New "LM-H2-Series" Linear Servomotors

Authors: *Kazuhiko Kato** and *Kouki Naka***

In the fields of semiconductor/LCD manufacturing equipment and mounters, there has been growing demand for enhanced precision, increased speed, improved efficiency and the like. To meet these demands, we have developed a new linear servomotor series called "LM-H2" that facilitates the construction of systems that combine high speed, high acceleration and high precision. This paper describes the downsizing and performance-enhancing technologies which we have developed and built into our "LM-H2-series" general-purpose linear servomotors, along with our motor-manufacturing technologies designed to flexibly meet a wide range of customer needs.

1. Features of Linear Servomotors

A linear servomotor consists of a primary side and a secondary side (see Fig. 1). Thrust is produced between the primary and secondary sides by applying current to the primary-side winding. The thrust can thus be obtained directly from the motor. Figure 2 compares the construction of a ball-screw-driven system and a linear servomotor-driven system. The linear servomotor-driven system possesses the distinctive feature of direct drive which directly moves an object to be moved and is capable of high speed and rapid acceleration/deceleration drive. Furthermore, the linear servomotor-driven system makes it possible to build high-precision drive systems that do not develop responsivity errors caused by backlash and friction, both of which are problems found in ball screws and couplings.

However, since such high-precision drive systems are built-in-structures within equipment, the motor size directly affects the dimensions of equipment, so it is necessary to offer size variations in order to permit selection of motors best suited to specifications imposed on such equipment. The motor must also be installed close to the object to be driven, so the heat given off by the motor can degrade the precision due to thermal expansion of the equipment. Therefore, physical downsizing and low heat generation are mandatory when designing linear servomotors.

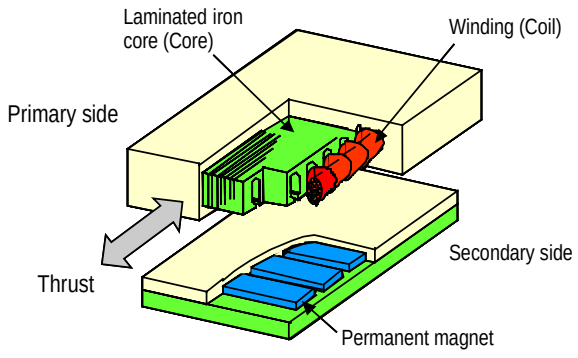

Fig. 1 Structures of linear servomotor

2. Building Block Method

In order to satisfy the above-mentioned specification requirements, we have adopted a building block method.

In the building block method, modular cores are arranged in an array with the required numbers of rows and columns as shown in Fig. 3 and teeth, each of which is furnished with a winding, are arranged likewise. These are then tied together with binding members for assembly into an integrated primary side. With this method, it is possible to form primary sides of various sizes using modular cores of the same size.

3. Winding Structure

Using the construction discussed in the preceding section, we studied the winding structure to take full advantage of the features of the construction.

In the case of distributed winding structures adopted in conventional motor series, it is difficult to downsize the coil ends of windings (see Fig. 4 (a)).

These coil-end portions do not contribute to the generation of thrust but give off heat (copper loss) produced by the resistance of the windings, so they should be made as small as possible. In addition, since it is also

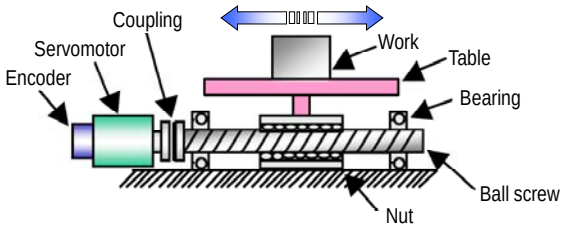

(a) Ball-screw-driven system

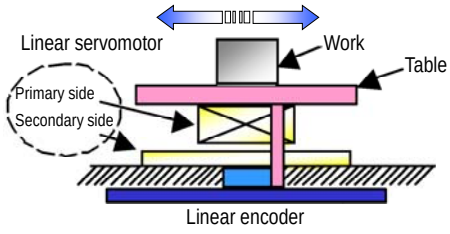

(b) Linear servomotor-driven system

Fig. 2 Drive systems by ball screw and linear servomotor

*Nagoya Works **Advanced Technology R&D Center

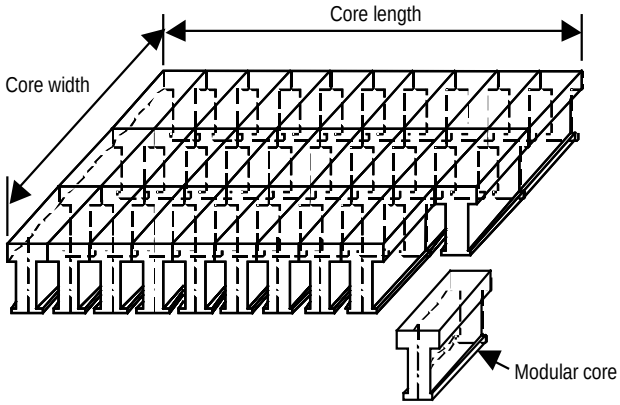

Fig. 3 Building block method core structure

difficult to dramatically improve the winding space factor (which is the ratio of the cross-sectional area of the winding to that of the slot in which the winding sits), it is hard to significantly reduce heat generation.

In the present development work, we adopted the concentrated winding structure shown in Fig. 4 (b) to solve the above-mentioned problem. In the concentrated winding structure, a winding is provided directly on the core block, making it possible to minimize the dimensions of the coil ends, and also significantly increase the space factor by making regular windings in slots. A 50% reduction in coil-end dimensions and a 70% increase in winding space factor have reduced both the physical size and heat generation, which are mutually contradictory, on the primary side of the motor.

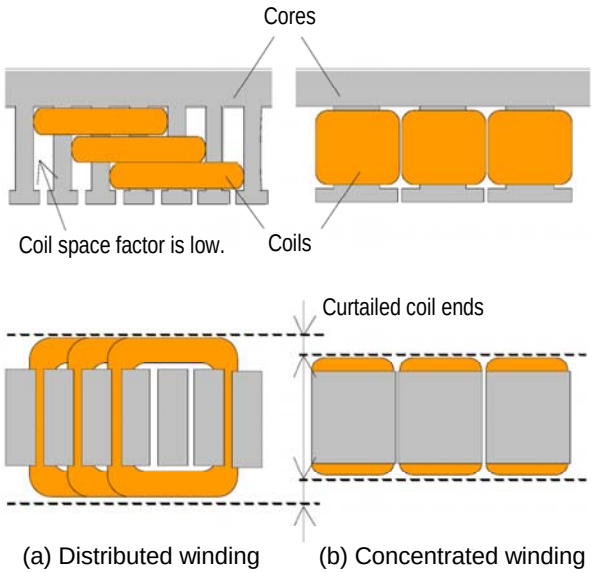

Fig. 4 Winding structure comparison between distribution winding and concentrated winding

4. Elimination of Skew

For high-precision transport, it is necessary to reduce cogging thrust, which is the thrust ripples that develop when the primary-side iron cores travel over the secondary-side magnets and reduces the positioning accuracy as well as the smoothness of transport. To reduce cogging, a skew structure such as shown in Fig. 5 is generally adopted. In the one shown in Fig. 5 (a), iron cores are laminated such that the iron-core array is skewed with each core shifted in the lengthwise direction little by little. Therefore, the length of the primary side becomes longer according to the amount of skew.

In the case of the skew structure on the secondary side, magnets are positioned in a slanting direction as shown in Fig. 5 (b). The skew angle varies depending on the motor series (core width). When rectangular magnets are to be used to increase the commonality of parts, some extra space is required in the direction of the width of the motor. Moreover, for producing the required torque, it is necessary to machine the mounting seats (yokes) in a parallelogram shape so that multiple secondary sides may be combined.

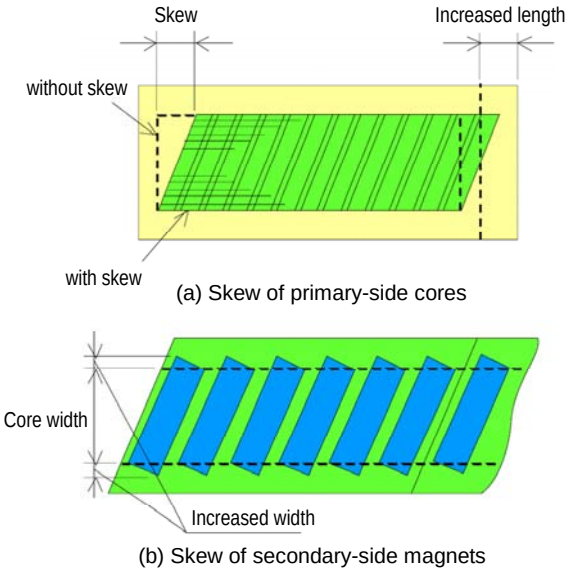

Fig. 5 Skew structure

In addition, a skew structure can degrade the thrust characteristics with respect to the current. Therefore, for our prototype under development, we optimized the core and magnet shapes using high-precision magnetic-field analysis technology, and implemented anti-cogging measures without skew on both the primary and secondary sides. In this way, we reduced the cogging torque while maintaining small size and low heat generation.

5. New "LM-H2-Series" Linear Servomotors

The lineup of LM-H2 series of linear servomotors developed this time extends up to 2400 N thrust as standard. Compared with our conventional series, this model lineup offers a broader selection in the upper reaches of the thrust scale.

Figure 6 compares the characteristics of a model from the conventional LM-H series and a model from the newly developed LM-H2 series, both rated at a maximum thrust of 600 N.

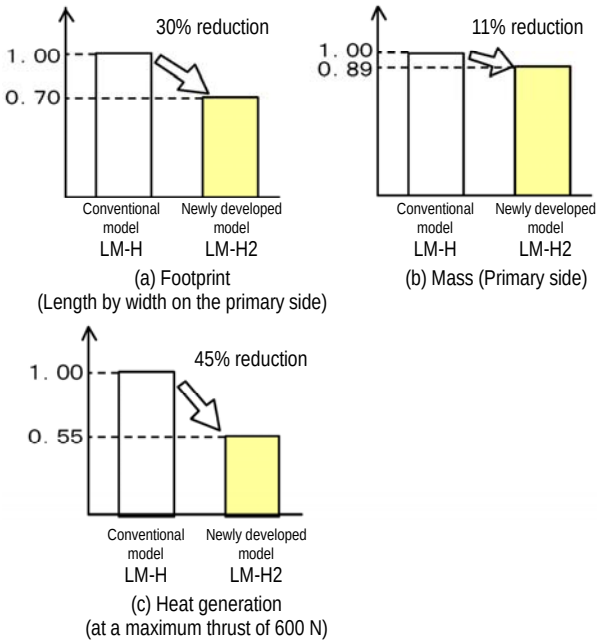

Fig. 6 Characteristic comparison (conventional model = 1.0)

The LM-H2-series model offers considerable performance improvements over its LM-H-series counterpart.

6. Conclusion

By adopting the building block method, the LM-H2 series allows flexible manufacturing of a wide range of linear servomotors in varying batch sizes. Furthermore, by increasing the density of windings and optimizing core and magnet geometries using the magnetic-field analysis technology, we have considerably reduced the physical size and heat generation compared with the earlier series. In future, we will deploy these new technologies to other series and models while further improving the performance.


MITSUBISHI ELECTRIC CORPORATION